

Document downloaded from:

<http://hdl.handle.net/10251/125667>

This paper must be cited as:

Steward, J.L.; Roman, J.E.; Lamas Daviña, A.; Aksoy, A. (2018). Parallel Direct Solution of the Covariance-Localized Ensemble Square Root Kalman Filter Equations with Matrix Functions. *Monthly Weather Review*. 146(9):2819-2836. <https://doi.org/10.1175/MWR-D-18-0022.1>



The final publication is available at

<http://doi.org/10.1175/MWR-D-18-0022.1>

Copyright American Meteorological Society

Additional Information

1 **Parallel Direct Solution of the Covariance-Localized Ensemble Square-Root**  
2 **Kalman Filter Equations with Matrix Functions**

3 Jeffrey L. Steward\*

4 *University of California Los Angeles, Los Angeles, California, United States*

5 Jose E. Roman

6 *Universitat Politècnica de València, València, Spain*

7 Alejandro Lamas Daviña

8 *Universitat Politècnica de València, València, Spain*

9 Altuğ Aksoy

10 *(1) Cooperative Institute for Marine and Atmospheric Studies, University of Miami, Miami,*  
11 *Florida, United States, (2) Hurricane Research Division, NOAA/AOML, Miami, Florida, United*  
12 *States*

13 \*Corresponding author address: Joint Institute for Regional Earth Science and Systems Engineer-  
14 ing, University of California, Los Angeles, Los Angeles, California, United States

15 E-mail: [jsteward@jifresse.ucla.edu](mailto:jsteward@jifresse.ucla.edu)

## ABSTRACT

16 Recently, the serial approach to solving the Square-Root Ensemble Kalman  
17 Filter (ESRF) equations in the presence of covariance localization was found  
18 to depend on the order of observations. As shown previously, correctly updat-  
19 ing the localized posterior covariance in serial requires additional effort and  
20 computational expense. A recent work, Steward et al. (2017), details an all-  
21 at-once direct method to solve the ESRF equations in parallel. This method  
22 uses the eigenvectors and eigenvalues of the forward observation covariance  
23 matrix to solve the difficult portion of the ESRF equations. The remaining  
24 assimilation is easily parallelized, and the analysis does not depend on the  
25 order of observations. While this allows for long localization lengths that  
26 would render local analysis methods inefficient, in theory an eigenpair-based  
27 method scales as the cube number of observations, making it infeasible for  
28 large numbers of observations. In this work, we extend this method to use  
29 the theory of matrix functions to avoid eigenpair computations. The Arnoldi  
30 process is used to evaluate the covariance localized ESRF equations on the  
31 reduced-order Krylov subspace basis. This method is shown to converge  
32 quickly and apparently regains a linear scaling with the number of obser-  
33 vations. The method scales similarly to the widely-used serial approach of  
34 Anderson and Collins (2007) in wall-time but not in memory usage. To im-  
35 prove the memory usage issue, this method potentially can be used without an  
36 explicit matrix. In addition, hybrid ensemble and climatological covariances  
37 can be incorporated.

## 38 **1. Introduction**

39 Data assimilation of increasingly plentiful satellite and radar observations requires efficient and  
40 accurate algorithms. A single overpass of a polar orbiting satellite over a regional numerical  
41 weather prediction (NWP) domain can produce tens of thousands of potentially usable observa-  
42 tions, especially when all-sky observations are considered. The Japanese K computer assimilates  
43 radar observations every 30 seconds with a 100-m grid spacing (Miyoshi et al. 2016), and with  
44 the next generation GOES-16 (Schmit et al. 2016) and Himawari 8 (Bessho et al. 2016) geosta-  
45 tionary observing platforms providing observations with approximately kilometer resolution ap-  
46 proximately every 5 minutes, data assimilation algorithms need to handle increasingly large data  
47 volumes to keep pace. In this paper we describe a new, efficient, and parallel technique for solving  
48 the covariance-localized Square-Root Ensemble Kalman Filter equations that overcomes several  
49 issues in previously described implementations.

50 The Ensemble Kalman Filter, first introduced in Evensen (1994), is one of the most widely used  
51 methods for data assimilation. Using an ensemble with a relatively small number of members  
52 to estimate the flow-dependent background error covariance from the Kalman filter as originally  
53 formulated (Kalman 1960) made it feasible to run statistical data assimilation problems even on  
54 very large domains. However, two main issues became apparent in the implementation of the  
55 Ensemble Kalman Filter. The first is that using the same observations to update the mean and  
56 ensemble perturbations leads to a systematic underestimation of covariance. Secondly, the unlo-  
57 calized estimated covariances contain sample error due to the low number of ensemble members  
58 used, leading to spurious relationships.

59 The issue of systematic covariance underestimation was first solved by perturbing observations  
60 with independently sampled noise for each ensemble member (Houtekamer and Mitchell 1998;

61 Burgers et al. 1998). While this solves the underestimation of covariance, adding additional noise  
62 increases sampling error, causing the filter to be suboptimal especially when the ensemble size  
63 is small (Whitaker and Hamill 2002). Subsequently, the Ensemble Square-Root Filter (ESRF)  
64 was introduced that corrects for the under-representation of error covariance by adding a square-  
65 root term to the Kalman update for the ensemble. Various flavors of ESRF have been developed  
66 (Bishop et al. 2001; Anderson 2001; Whitaker and Hamill 2002), which Tippett et al. (2003)  
67 showed are all equivalent in the sense they perform analysis in the same vector space and find  
68 the same covariance. These methods as originally formulated assume the rank of the covariance  
69 matrices is the number of ensemble members.

70 Independently from covariance underestimation, the issue of spurious correlations due to small  
71 ensemble size has been addressed in two main ways: covariance localization and local analysis.  
72 Sakov and Bertino (2011) demonstrated that these two approaches are approximately equal, and  
73 the choice of approach is therefore dependent upon other factors. Critically, the localization ra-  
74 dius used in local methods will determine their efficiency, and large localization radii will require  
75 repetitive solution of large problems for each grid point. In this work we investigate covariance  
76 localization, which uses a Schur product (component-wise multiplication) to zero out correlations  
77 further than a specified distance (Gaspari and Cohn 1999; Houtekamer and Mitchell 2001; Hamill  
78 et al. 2001). This causes the rank of the forward-observation-covariance matrix used in the inverse  
79 of the Kalman gain to increase beyond the number of ensemble members. As shown in Steward  
80 et al. (2017), a relatively short localization radius will lead to a full-rank forward-observation-  
81 covariance matrix, while a long localization radius will lead to a rank deficient one.

82 The combination of these factors leads to several different possibilities for scalable parallel im-  
83 plementations of the Ensemble Kalman filter equations. Local methods with perturbed obser-  
84 vations and covariance localization include Keppenne and Rienecker (2002); Houtekamer et al.

85 (2013); Bishop et al. (2015); Nino-Ruiz et al. (2015), while local analysis methods based on the  
86 ESRF equations include Ott et al. (2002); Anderson (2003); Zhang et al. (2005); Hunt et al. (2007);  
87 Wang et al. (2013); Nino-Ruiz et al. (2017). Note that the widely used Local Ensemble Kalman  
88 Transform Filter of Hunt et al. (2007, LETKF) applies a localization strategy based on the ob-  
89 servation error covariance matrix  $\mathbf{R}$  rather than on the sample covariance matrices estimated by  
90 the ensemble. The widely-used and highly efficient method of Anderson and Collins (2007) is a  
91 “global” analysis (i.e. non-local) parallel implementation based on the serial assimilation of the  
92 ESRF equations with covariance localization. This method also treats the observations as part of  
93 an augmented state in order to update the observations in parallel without requiring excessive com-  
94 munication. Houtekamer and Mitchell (2001) describes a global analysis method with perturbed  
95 observations and covariance localization.

96 Due to the difficulties in solving the global ESRF equations directly, in implementations such as  
97 Anderson (2001), Whitaker and Hamill (2002), Anderson and Collins (2007) and Aksoy (2013)  
98 a serial approach is utilized where a single observation is assimilated at a time. This approach  
99 is provably identical to the global analysis without covariance localization and linear observation  
100 operators. However, with covariance-based localization, the ordering of observations affects the  
101 analysis as shown in Nerger (2015) and Bishop et al. (2015) due to the nonlinear nature of co-  
102 variance localization. In other words, in the presence of ensemble sample covariance localization,  
103 serially assimilating observation  $A$  before observation  $B$  may give different results than assimilat-  
104 ing observation  $B$  before  $A$ . The magnitude of this issue has not yet been fully explored.

105 As shown in Bishop et al. (2015), the issue of observation-ordering dependent analysis in serial  
106 covariance localized methods stems from the inconsistent application of the high-rank localized  
107 covariance matrices. In particular, when covariance localization is used, the matrix to invert in  
108 the Kalman gain becomes full rank or nearly full-rank as shown in e.g. Steward et al. (2017).

109 Without covariance localization (or in a local analysis method that does not increase the rank of  
110 the matrix using a Schur product), as shown in Tippett et al. (2003), the Sherman Woodbury update  
111 is sufficient for an unlocalized matrix as the rank of the matrix is at most the number of ensemble  
112 members (Godinez and Moulton 2012). However, the fundamental shift to high-rank matrices  
113 requires additional effort to correct.

114 Several strategies have been proposed to handle this observation-ordering dependence within a  
115 serial filter. Bishop et al. (2015) proposes the Consistent Hybrid Ensemble Filter (CHEF) with  
116 local analysis and perturbed observations that will ensure the analysis is consistent and does not  
117 depend on the order of assimilation. Kotsuki et al. (2017) presents a study of observation ordering  
118 with a Lorenz-96 model and investigates rules for observation assimilation ordering to minimize  
119 analysis forecast error. The method of correcting sample correlation described in Anderson (2012)  
120 has also been used to reduce the dependence of observation ordering in a serial filter (J. Anderson  
121 2017, personal communication).

122 Extending upon these works, as an alternative to attempting to apply and update the high-rank  
123 localized matrices serially in a consistent way, we propose assimilating all observations within the  
124 assimilation window in a single pass as a potential alternative. In other words, we do not utilize  
125 the single observation processing strategy normally employed for serial filter solutions and instead  
126 solve the ESRF equations directly. This is done by dividing the necessary matrix operators across  
127 the set of processing elements in a “top-down” fashion as opposed to the “bottom-up” approach  
128 of local analysis. This method was utilized in Steward et al. (2017) (hereafter S17) to provide a  
129 global, “all-at-once,” parallel, direct solution of the covariance-localized ESRF equations. Note  
130 that “all-at-once” here is used to refer to assimilating all observations that the serial filter would  
131 assimilate one-by-one but not all observations within all assimilation windows at once, i.e. the  
132 method in S17 as well as the one presented below are both sequential filters in that batches of

133 observations can also be assimilated. The benefit of this approach is that the analysis consistently  
134 applies the high-rank covariance-localized matrices and, as a result, does not depend on the order  
135 of observations. It provides a solution to the ESRF equations with a proven error bounds that can  
136 be used as a benchmark against other methodologies.

137 The cost of this approach is that a product with the entire full-rank matrix inverse (which also  
138 requires a square-root term) of the forward observation error covariance is required. S17 solves  
139 for eigenvalues and eigenvectors of the observation covariance matrix and uses the ESRF matrix  
140 function “scalarized” on the eigenvalues to find the required matrix inverses and products. As  
141 eigenpairs are extremely convenient for mathematical analysis, the approach in S17 also includes  
142 an error bounds related to the smallest eigenvalue used. The final analysis is also shown not to  
143 depend on the ordering of observations. This error-bounded method, which directly solves the  
144 ESRF equations, is therefore a highly accurate solution to the ESRF equations known to be the  
145 minimum variance solution to the data assimilation problem.

146 However, as predicted by theory and shown in this work, while the method described in S17 is  
147 accurate to within a configurable tolerance, it is impractical for large numbers of observations due  
148 to the nature of the eigenproblem, where for general matrices finding a large number of eigen-  
149 pairs scales as  $O(n^3)$  for a matrix of size  $n \times n$  (Golub and Van Loan 1996).  $n$  is the number  
150 of quality-controlled observations in this case. This paper extends S17 to take advantage of re-  
151 cent improvements in the theory and computation of matrix functions to transform the problem  
152 of solving the difficult inverse and square-root portion of the ESRF equations into to computing  
153 matrix-vector products that are used to build up a Krylov subspace and, through a library call, ap-  
154 plying the matrix function directly to a small dense matrix. This small dense matrix represents the  
155 compression of the larger localized forward-observation covariance matrix onto the reduced-order  
156 Krylov subspace basis.



157 As we show below, this matrix function method gives results that are practically identical to the  
158 error-bounded methodology of S17 but is much more computationally efficient. As only a matrix-  
159 vector product with the observation covariance matrix is required, this matrix function approach is  
160 well-suited for a matrix-free implementation where the covariance matrix is not explicitly formed.  
161 This method is also amenable to hybrid covariance models using both ensemble and climatological  
162 covariances.

163 We implement the matrix function method and compare the performance results with both S17 as  
164 well as the parallel augmented-state method of Anderson and Collins (2007), hereafter referred to  
165 as AC07. As a proof-of-concept application, we test this method on the difficult, highly-nonlinear  
166 case of first cycle tropical cyclone (TC) data assimilation. In this case, the background ensemble  
167 can contain position errors of features and the posterior analysis increment can be large (e.g. Chang  
168 et al. 2014). As we show, the order-dependence issue of a serial filter is non-trivial in this case.  
169 In order to demonstrate the unique properties of our new method, we investigate TC assimilation  
170 with a long covariance length-scale that would be impractical for local analysis methods. As we  
171 show, the matrix function method is roughly comparable in terms of wall-time performance to  
172 AC07 and far superior to S17. The analysis results do not depend on observation ordering like  
173 S17 but contrary to AC07. However, our results demonstrate the memory scaling of the matrix  
174 function method is inferior to AC07, and suggest that matrix-free methods would be required to  
175 scale this method to the order of millions of observations at once.

176 This paper is organized as follows. Section 2 summarizes S17 in order to build upon it. In section  
177 3, the eigenpair computation of S17 is replaced with a much more efficient matrix function based  
178 approach that uses a basis for the Krylov space to compress the forward observation covariance  
179 matrix and apply the covariance-localized ESRF matrix functions to this reduced-order matrix.  
180 Section 4 summarizes AC07. Section 5 presents numerical results of the matrix function approach

181 and a performance comparison to S17 and AC07. Finally, section 6 presents conclusions and a  
 182 discussion.

## 183 2. Eigenvalue/eigenvector solution of S17

184 In this section, we briefly review S17 in order to introduce the new matrix function method that  
 185 extends it. Given an ensemble  $\mathbf{X}_f$  of a previous forecast, the updated analysis to the ensemble  
 186 mean  $\bar{\mathbf{x}}_f$  of size  $N_{\text{state}} \times 1$  and ensemble perturbations  $\mathbf{X}'_f$  of size  $N_{\text{state}} \times N_{\text{ens}}$ , the square-root  
 187 Ensemble Kalman filter without perturbed observations (Whitaker and Hamill 2002) is:

$$\begin{aligned}\bar{\mathbf{x}}_a &= \bar{\mathbf{x}}_f + \mathbf{K} \left( \mathbf{y} - \overline{H(\mathbf{X}_f)} \right), \\ \mathbf{X}'_a &= \mathbf{X}'_f + \tilde{\mathbf{K}} (\mathbf{0} - H\mathbf{X}),\end{aligned}\tag{1}$$

188 where  $\mathbf{y}$  ( $N_{\text{obs}} \times 1$ ) are the observations,  $\overline{H(\mathbf{X}_f)}$  ( $N_{\text{obs}} \times 1$ ) is the mean of the forward-calculated  
 189 observation operators, and  $H\mathbf{X}_{i,j} = h_i \left( \mathbf{X}_f^{(j)} \right) - \overline{h_i(\mathbf{X}_f)}$  is the mean-subtracted  $i^{\text{th}}$  observation op-  
 190 erator acting on the  $j^{\text{th}}$  ensemble member  $\mathbf{X}_f^{(j)}$ .  $H\mathbf{X}$  is  $N_{\text{obs}} \times N_{\text{ens}}$  (as is  $\mathbf{0}$ , a matrix filled with  
 191 zeros). The traditional Kalman gain,  $\mathbf{K}$  ( $N_{\text{state}} \times N_{\text{obs}}$ ), is

$$\mathbf{K} = \mathbf{C}_{\mathbf{x},H\mathbf{x}} \mathbf{D}^{-1},\tag{2}$$

192 where  $\mathbf{C}_{\mathbf{x},H\mathbf{x}} = \text{cov}(\mathbf{x}_f, H(\mathbf{x}_f))$  is the localized covariance between  $\mathbf{x}_f$  (an  $N_{\text{state}} \times 1$  random vari-  
 193 able representing the previous forecast) and  $H(\mathbf{x}_f)$  (the observation operator acting on this random  
 194 variable).  $\mathbf{D} = \mathbf{C}_{H\mathbf{x},H\mathbf{x}} + \mathbf{R}$  for  $\mathbf{C}_{H\mathbf{x},H\mathbf{x}} = \text{cov}(H(\mathbf{x}_f), H(\mathbf{x}_f))$ , the localized forward observation  
 195 covariance, and  $\mathbf{R}$  is the observation error covariance  $\text{cov}(\mathbf{y}_t - H(\mathbf{x}_f))$  for a random variable  $\mathbf{y}_t$   
 196 representing the true observations without observation noise.

197  $\tilde{\mathbf{K}}$  ( $N_{\text{state}} \times N_{\text{obs}}$ ), the correction from using non-perturbed observations, is

$$\tilde{\mathbf{K}} = \mathbf{C}_{\mathbf{x},H\mathbf{x}} \mathbf{D}^{-1/2} \left( \sqrt{\mathbf{D}} + \sqrt{\mathbf{R}} \right)^{-1}.\tag{3}$$

198 As detailed in S17, the covariance matrices we consider can include localized-ensemble  
 199 based correlations in observation space and/or variational-style model-space localization. For  
 200 observation-space localization, a component-wise multiplication  $\circ$  between two matrices is used  
 201 as

$$\mathbf{C}_{H\mathbf{x},H\mathbf{x}}^{\text{obs}} = \rho_{\mathbf{y},\mathbf{y}} \circ \mathbf{Q}_{H\mathbf{x},H\mathbf{x}} \quad (4)$$

202 where  $\rho_{\mathbf{y},\mathbf{y}}$  is the localization matrix arising from a localization function (Gaspari and Cohn 1999)  
 203  $\ell$  such that

$$(\rho_{\mathbf{y},\mathbf{y}})_{i,j} = \ell(d_{i,j}|L_{i,j}) \quad (5)$$

204 where  $d_{i,j}$  is the distance between the location of the  $i^{\text{th}}$  and  $j^{\text{th}}$  observation, and  $L_{i,j}$  is the charac-  
 205 teristic length scale for the localization function  $\ell$ .  $\mathbf{Q}_{H\mathbf{x},H\mathbf{x}}$  is the sample covariance matrix

$$\mathbf{Q}_{H\mathbf{x},H\mathbf{x}} = \frac{H\mathbf{X}(H\mathbf{X})^{\text{T}}}{N_{\text{ens}} - 1}. \quad (6)$$

206 Likewise, the observation-space localized model and observation cross-covariance is given by

$$\mathbf{C}_{\mathbf{x},H\mathbf{x}}^{\text{obs}} = \rho_{\mathbf{x},\mathbf{y}} \circ \mathbf{Q}_{\mathbf{x},H\mathbf{x}} \quad (7)$$

207 for

$$(\rho_{\mathbf{x},\mathbf{y}})_{i,j} = \ell(d_{i,j}|L_{i,j}) \quad (8)$$

208 where  $d_{i,j}$  is the distance between the location of the model state  $i$  and observation  $j$  with the same  
 209 localization function as equation (5), and

$$\mathbf{Q}_{\mathbf{x},H\mathbf{x}} = \frac{\mathbf{X}'_f(H\mathbf{X})^{\text{T}}}{N_{\text{ens}} - 1} \quad (9)$$

210 As noted in Campbell et al. (2010), integrated observations such as satellite scans do not have a  
 211 particular vertical location to ascribe. In these cases, model-space localization is more applicable.  
 212 For model-space localization, the observation operator tangent-linear  $\mathbf{H}$  and adjoint  $\mathbf{H}^{\text{T}}$  are applied

213 to the localized model covariance as

$$\mathbf{C}_{H\mathbf{x},H\mathbf{x}}^{\text{model}} = \mathbf{H}(\rho_{\mathbf{x},\mathbf{x}} \circ \mathbf{Q}_{\mathbf{x},\mathbf{x}}) \mathbf{H}^T \quad (10)$$

214 where

$$\mathbf{Q}_{\mathbf{x},\mathbf{x}} = \frac{\mathbf{X}'_f (\mathbf{X}'_f)^T}{N_{\text{ens}} - 1} \quad (11)$$

215 for the ensemble perturbations  $\mathbf{X}'_f$ , and

$$(\rho_{\mathbf{x},\mathbf{x}})_{i,j} = \ell(d_{i,j}|L_{i,j}) \quad (12)$$

216 where  $d_{i,j}$  is the distance between the location of two model states  $i$  and  $j$  with the same localiza-  
 217 tion function as equation (5). Equation (7) is changed analogously as

$$\mathbf{C}_{\mathbf{x},H\mathbf{x}}^{\text{model}} = (\rho_{\mathbf{x},\mathbf{x}} \circ \mathbf{Q}_{\mathbf{x},\mathbf{x}}) \mathbf{H}^T \quad (13)$$

218 Note that all of these localized matrices are sparse, and zero elements (i.e. the correlations farther  
 219 than the specified localization distance) are not stored in memory or computed. Thus, for example,  
 220 only those elements of  $\mathbf{Q}_{H\mathbf{x},H\mathbf{x}}$  that will be non-zero after localization are calculated. Furthermore,  
 221 the full model-space matrix  $\mathbf{Q}_{\mathbf{x},\mathbf{x}}$  will never be explicitly formed due to its prohibitively large size.  
 222 See S17 for more detail.

223 As we will allow for full-rank matrices, our method is compatible with either of these local-  
 224 ization methods, a linear combination of the two, or any other “reasonable” modeled covariance  
 225 between  $H\mathbf{x}$  and  $H\mathbf{x}$  and  $\mathbf{x}$  and  $H\mathbf{x}$ , which we denote in general  $\mathbf{C}_{H\mathbf{x},H\mathbf{x}}$  and  $\mathbf{C}_{\mathbf{x},H\mathbf{x}}$ . Note that in  
 226 this work we only present results for the observation-based localization of equations (4) and (7),  
 227 however.

228 We now return to solving equation (1). Both S17 and the matrix function approach utilize a  
 229 pre-processing step of a transformation first introduced in Bishop et al. (2001) to whiten the ob-  
 230 servations as  $\mathbf{y} = \mathbf{R}_{\text{old}}^{-1/2} \mathbf{y}_{\text{old}}$ , where the “old” subscript represents the untransformed observations.

231 The observation operator is also scaled as  $H(\mathbf{x}) = \mathbf{R}_{\text{old}}^{-1/2} H_{\text{old}}(\mathbf{x})$ . As a result of this pre-processing  
 232 transformation, the  $\mathbf{R}$  matrix is now identity, which makes equation (3) much easier to solve. For  
 233 the diagonal observation error matrix  $\mathbf{R}_{\text{old}}$  typically used in data assimilation (which assumes un-  
 234 correlated observation errors), multiplying by  $\mathbf{R}_{\text{old}}^{-1/2}$  is equivalent to dividing each observation  
 235 by the standard deviation of the observation error, and for non-diagonal  $\mathbf{R}_{\text{old}}$ , this transformation  
 236 removes that off-diagonal correlation using principal components.

237 As  $\mathbf{D}_{\text{new}} = \mathbf{C}_{H\mathbf{x},H\mathbf{x}} + \mathbf{I}$  by this transformation (note that we drop the “new” subscript in what  
 238 follows as it could be applied to virtually all matrices; i.e. we write  $\mathbf{D}_{\text{new}}$  as  $\mathbf{D}$  in a slight abuse of  
 239 notation), this leads to

$$\tilde{\mathbf{K}} = \mathbf{C}_{\mathbf{x},H\mathbf{x}} \mathbf{M}^{-1} \quad (14)$$

240 for  $\mathbf{M} = \mathbf{D} + \sqrt{\mathbf{D}}$ . Let  $\lambda_i, \mathbf{v}_i$  denote the  $i^{\text{th}}$  eigenpair of  $\mathbf{C}_{H\mathbf{x},H\mathbf{x}}$ . Then

$$\mathbf{M}\mathbf{v}_i = \mathbf{C}_{H\mathbf{x},H\mathbf{x}} \mathbf{v}_i + \mathbf{v}_i + (\mathbf{C}_{H\mathbf{x},H\mathbf{x}} + \mathbf{I})^{1/2} \mathbf{v}_i. \quad (15)$$

241 As shown in S17, we have

$$\mathbf{M}\mathbf{v}_i = \left( \lambda_i + 1 + (\lambda_i + 1)^{1/2} \right) \mathbf{v}_i. \quad (16)$$

242 Therefore,

$$\mathbf{M}^{-1}\mathbf{v}_i = \lambda'_i \mathbf{v}_i \quad (17)$$

243 for

$$\lambda'_i = \frac{1}{\lambda_i + 1 + (\lambda_i + 1)^{1/2}}. \quad (18)$$

244 We find the largest  $r$  eigenvalues and corresponding eigenvectors of  $\mathbf{C}_{H\mathbf{x},H\mathbf{x}}$ , where  $r$  is chosen  
 245 such that  $\lambda_{r+1} \leq \varepsilon_\lambda$  for some small constant  $\varepsilon_\lambda$ , and we can therefore solve

$$\mathbf{M}^{-1}(\mathbf{0} - H\mathbf{X})_j \approx \sum_{i=1}^r \lambda'_i \alpha_{i,j} \mathbf{v}_i \quad (19)$$

246 for  $\alpha_{i,j} = -\mathbf{v}_i^T H\mathbf{X}_j$ . An error bound on this approximation related to  $\varepsilon_\lambda$  is proved in S17.

247 Similarly, for the mean update:

$$\mathbf{D}^{-1}(\mathbf{y} - \overline{H(\mathbf{X}_f)}) \approx \sum_{i=1}^r \frac{\beta_i}{\lambda_i + 1} \mathbf{v}_i, \quad (20)$$

248 where  $\beta_i = \mathbf{v}_i^T (\mathbf{y} - \overline{H(\mathbf{X}_f)})$ .

249 The  $N_{\text{obs}} \times N_{\text{ens}} + 1$  matrix  $(\mathbf{E}|\mathbf{g})$ , where

$$\mathbf{E}_j = \sum_{i=1}^r \lambda_i' \alpha_{i,j} \mathbf{v}_i \quad (21)$$

250 and

$$\mathbf{g} = \sum_{i=1}^r \frac{\beta_i}{\lambda_i + 1} \mathbf{v}_i, \quad (22)$$

251 is then distributed to all processing elements. The remaining Kalman gain from equation (1) only  
 252 requires multiplication with  $\mathbf{C}_{\mathbf{x},H\mathbf{x}}$ , which can proceed in an embarrassingly parallel fashion. This  
 253 makes an efficient parallel method that only requires the eigenpairs of the  $N_{\text{obs}} \times N_{\text{obs}}$ , sparse,  
 254 positive semi-definite symmetric matrix  $\mathbf{C}_{H\mathbf{x},H\mathbf{x}}$ . The Scalable Library for Eigenproblem Com-  
 255 putation (SLEPc, Hernandez et al. 2005), which is built upon the Portable Extensible Toolkit for  
 256 Scientific Computing (PETSc, Balay et al. 1997, 2016, 2017), is used to solve this eigenproblem  
 257 using sparse matrices in a manner that scales well as a function of the number of processors, as  
 258 shown in S17.

### 259 3. New matrix function approach

260 We first note that while S17 evaluates the largest  $r$  eigenpairs of  $\mathbf{C}_{H\mathbf{x},H\mathbf{x}}$  in order to solve equation  
 261 (1), only those eigenvectors  $i$  such that  $\alpha_{i,j} \neq 0$  for all  $j$  and  $\beta_i \neq 0$  are required. This suggests  
 262 a more efficient solution that does not require all eigenpairs. In this section we develop such a  
 263 solution that requires only the matrix-vector product  $\mathbf{C}_{H\mathbf{x},H\mathbf{x}} \mathbf{b}$  for some vector  $\mathbf{b}$  to compute a  
 264 reduced-order, accurate basis for representation of the ESRF matrix functions.

265 In addition to solving the eigenproblem, SLEPc can also evaluate the action of a matrix function  
 266 on a vector,  $\mathbf{z} = f(\mathbf{A})\mathbf{b}$  where  $\mathbf{z}$  and  $\mathbf{b}$  are vectors,  $\mathbf{A}$  is a matrix, and  $f$  is a matrix function in the  
 267 sense given in Higham (2008). In the case of the mean  $\mathbf{K}$  in equation (2) given above

$$f_1(\mathbf{D}) = \mathbf{D}^{-1}, \quad (23)$$

268 while for  $\tilde{\mathbf{K}}$  in equation (14),

$$f_2(\mathbf{D}) = (\mathbf{D} + \sqrt{\mathbf{D}})^{-1}. \quad (24)$$

269 Recall that  $\mathbf{D} = \mathbf{C}_{H\mathbf{x}, H\mathbf{x}} + \mathbf{I}$ . Also note that  $f_1$  involves the standard linear system of equations  
 270  $\mathbf{D}\mathbf{x} = \mathbf{b}$ , solving for  $\mathbf{x}$ , which is normally handled by other methods; in this work, we test using  
 271 the matrix function approach for both the mean and the perturbations.

272 The matrix function solvers in SLEPc are based on Krylov subspace methods (Higham 2008,  
 273 Ch. 13). Earlier works using Krylov subspace methods to approximate matrix functions in-  
 274 clude Van Der Vorst (1987), Saad (1992) and Hochbruck and Lubich (1997). These meth-  
 275 ods are appropriate for the case of our large, high-rank matrix  $\mathbf{D}$  as they compute the result  
 276  $\mathbf{z}$  without explicitly building the matrix  $f(\mathbf{D})$ . The calculation of  $f(\mathbf{D})\mathbf{b}$  proceeds in a man-  
 277 ner similar to the Arnoldi method (Arnoldi 1951) for finding eigenpairs. At the first step,  
 278  $\mathbf{V}_1 = \frac{\mathbf{b}}{\|\mathbf{b}\|_2}$ , and at step  $m$ , given an  $N_{\text{obs}} \times (m-1)$  orthonormal basis  $\mathbf{V}_{m-1}$  of the Krylov sub-  
 279 space  $\mathcal{H}_{m-1}(\mathbf{D}, \mathbf{b}) = \text{span}\{\mathbf{b}, \mathbf{D}\mathbf{b}, \mathbf{D}^2\mathbf{b}, \dots, \mathbf{D}^{m-2}\mathbf{b}\}$ , we seek the orthonormal basis  $\mathbf{V}_m$  that spans  
 280  $\mathcal{H}_m(\mathbf{D}, \mathbf{b})$ . This is done by the Arnoldi relation  $\mathbf{D}\mathbf{V}_{m-1} = \mathbf{V}_{m-1}\mathbf{H}_{m-1} + h_{m,m-1}\mathbf{v}_m\mathbf{e}_{m-1}^T$ , where  
 281  $\mathbf{H}_{m-1}$  is an  $(m-1) \times (m-1)$  upper Hessenberg matrix that contains the values of the projections  
 282 of  $\mathbf{D}$  onto the basis  $\mathbf{V}_{m-1}$ ,  $\mathbf{v}_m$  is the  $m^{\text{th}}$  column to be added to  $\mathbf{V}_m$  this iteration, and  $h_{m,m-1}$  is the  
 283  $(m, m-1)$  entry in the  $\mathbf{H}_m$  matrix.  $\mathbf{e}_{m-1}$  is the  $m-1$  unit coordinate vector, so  $h_{m,m-1}\mathbf{v}_m\mathbf{e}_{m-1}^T$  is  
 284 the  $N_{\text{obs}} \times (m-1)$  zero matrix except column  $m-1$  which is  $h_{m,m-1}\mathbf{v}_m$ . Once  $\mathbf{V}_m$  is found, the

285 approximation of  $\mathbf{z}$  can be computed as

$$\tilde{\mathbf{z}}_m = \beta \mathbf{V}_m f(\mathbf{H}_m) \mathbf{e}_1 \quad (25)$$

286 where  $\beta = \|\mathbf{b}\|_2$ .  $\mathbf{e}_1$  is the first coordinate vector, so right multiplying by it gives the first column  
287 of  $\beta \mathbf{V}_m f(\mathbf{H}_m)$  in equation (25). Note that  $\mathbf{b} = \beta \mathbf{V}_m \mathbf{e}_1$ . In addition, note that  $\mathbf{H}_m$  represents the  
288 compression of  $\mathbf{D}$  onto  $\mathcal{K}_m(\mathbf{D}, \mathbf{b})$  with respect to the basis  $\mathbf{V}_m$ . Hence, the problem of computing  
289 the function of a large matrix  $\mathbf{D}$  of order  $N_{\text{obs}}$  is reduced to computing the function of a small  
290 matrix  $\mathbf{H}_m$  of order  $m$  with  $m \ll N_{\text{obs}}$ . For the latter task, we can employ algorithms for dense  
291 matrices as discussed below.

292 Note that in the above description, the Arnoldi process requires a numerically stabilized Gram-  
293 Schmidt process to orthonormalize the basis vectors in a way that the final result is not overly af-  
294 fected by numerical noise. Furthermore, the parallelization of this stabilized process requires care-  
295 ful implementation to avoid negatively impacting performance by creating bottlenecks. Thus, the  
296 relatively straight-forward (conceptually) Gram-Schmidt process becomes rather complex when  
297 implemented in a parallel setting as discussed in Björck (1994) and Frayssé et al. (1998). SLEPc  
298 utilizes an efficient parallel version of the Iterated Classical Gram-Schmidt (ICGS) in the Arnoldi  
299 process that does not require global communication but maintains numerical stability. As in the  
300 high-level description given above, the resulting projections in the ICGS process onto the previous  
301 basis vectors are stored in the  $\mathbf{H}_m$  matrix. For more details on the orthogonalization process in  
302 SLEPc, see Hernandez et al. (2007).

303 The  $m$  parameter is of paramount importance for this method. If  $m$  is too small the Krylov sub-  
304 space will not contain enough information to build an accurate approximation. On the other hand,  
305 if  $m$  is too large, the memory requirements for storing  $\mathbf{V}_m$  (as well as the computational cost) will  
306 be prohibitive. For this reason, SLEPc implements a restarted variant of the method, where  $m$  is



307 prescribed to a fixed value; here we use  $m = 150$ , which as shown below is based on testing for our  
308 particular application. When the subspace reaches this size, a restart is carried out by keeping part  
309 of the data computed so far and discarding unnecessary information. Investigation into restarting  
310 matrix function iterations is still an area of active research (Afanasjew et al. 2008; Eiermann et al.  
311 2011; Frommer et al. 2017). SLEPc implements the Eiermann-Ernst restart (Eiermann and Ernst  
312 2006), in which only the last basis vector  $\mathbf{v}_{m+1}$  is kept (in order to continue the Arnoldi recur-  
313 rence) along with the matrix  $\mathbf{H}_m$  that is “glued” together with the previous ones. After  $k$  restarts,  
314 the matrix used in the approximation (25) has the form

$$\mathbf{H}_{km} = \begin{bmatrix} \mathbf{H}_{(k-1)m} & \mathbf{0}_m \\ h_{m+1,m}^{(k-1)} \mathbf{e}_1 \mathbf{e}_{(k-1)m}^T & \mathbf{H}_m^{(k)} \end{bmatrix}, \quad (26)$$

315 where  $\mathbf{H}_m^{(k)}$  is the matrix computed by the Arnoldi method in the  $k^{\text{th}}$  restart. Note that in the  
316 Eiermann-Ernst restart, the glued matrix (26) is not used directly in (25) because  $\mathbf{H}_{km}$  has size  $km \times$   
317  $km$  but  $\mathbf{V}_m$  has only  $m$  columns. Therefore, only the last  $m$  components of the vector  $f(\mathbf{H}_{km})\mathbf{e}_1$  are  
318 used in (25) to give a correction to be added to the approximation available in the previous restart.  
319 This correction is given by  $\tilde{\mathbf{z}}^{(k)} = \tilde{\mathbf{z}}^{(k-1)} + \mathbf{c}^{(k)}$ , where

$$\mathbf{c}^{(k)} = \beta \mathbf{V}_m^{(k)} [\mathbf{0}, \mathbf{I}_m] f(\mathbf{H}_{km}) \mathbf{e}_1, \quad (27)$$

320 and  $\mathbf{V}_m^{(k)}$  is the basis computed in the last restart. Equations (25) through (27) are implemented in  
321 a numerically efficient way in SLEPc.

322 SLEPc bases the stopping criterion on the norm of the correction, i.e. restarting continues until  
323  $\|\mathbf{c}^{(k)}\|_2 < \beta \cdot \varepsilon_{\text{tol}}$  for some user-defined  $\varepsilon_{\text{tol}}$  ( $10^{-8}$  by default for 8-byte floating point precision).  
324 As noted in Eiermann and Ernst (2006), the Arnoldi method converges rapidly with superlinear  
325 behavior for smooth functions. The convergence behavior when including restarting is presented  
326 in Afanasjew et al. (2008) for a related method.

327 In this work, we are interested in solving  $\mathbf{g} = f_1(\mathbf{D})(\mathbf{y} - \overline{H(\mathbf{X}_f)})$  to replace equation (22) and  
 328  $\mathbf{E}_j = f_2(\mathbf{D})(\mathbf{0} - H\mathbf{X})_j$  to replace equation (21) for  $j = 1, \dots, N_{\text{ens}}$ . Applying the method described  
 329 above leads to the evaluation of  $f_1(\mathbf{H}_1)$  and  $f_2(\mathbf{H}_2)$  explicitly for small dense matrices  $\mathbf{H}_1$  and  $\mathbf{H}_2$   
 330 of the form in eq. (26). Note that these matrices are not symmetric even though  $\mathbf{D}$  is symmetric,  
 331 and also note that the matrices grow at each restart of the Krylov method.

332 SLEPc allows flexibility in the definition of functions by combining two simpler functions. In  
 333 our case, we define  $f_1(\cdot)$  as the reciprocal of the identity function and  $f_2(\cdot)$  as the reciprocal of  
 334 another function, which in turn is defined as the sum of two functions (identity and the square root).  
 335 All these sub-functions can be evaluated easily except the matrix square root. For this SLEPc  
 336 implements a reduction to (real) Schur form followed by a block version of a Schur algorithm  
 337 (Higham 1987; Deadman et al. 2012).

338 Note that only the matrix action  $\mathbf{D}\mathbf{b}$  is required in this algorithm, allowing for matrix-free imple-  
 339 mentations. This could be potentially useful for defining matrix-vector products using the “mod-  
 340 ulation product” defined in Bishop and Hodyss (2009) or for variational-style covariances that  
 341 use Fast Fourier Transforms (FFT) to define the action of a circulant covariance matrix. Hybrid  
 342 methods are also possible; as long as the action of the covariance  $\mathbf{C}_{H\mathbf{x}, H\mathbf{x}}$  as well as  $\mathbf{C}_{\mathbf{x}, H\mathbf{x}}$  can be  
 343 applied, any such modeled covariance can be imposed on the analysis through the ESRF equations  
 344 through this approach.

#### 345 **4. Serial augmented-state filter of AC07**

346 In order to compare the performance of our new matrix function approach to an existing method,  
 347 we briefly summarize the method of AC07 here. AC07 details a highly scalable approach to  
 348 solving the ESRF equations in serial that is provably identical to the global solution with linear  
 349 observation operators and without covariance localization. With covariance localization, however,

350 the results will depend upon the ordering of observations as discussed above, although to what  
 351 extent this difference will impact ensemble NWP forecasts has not yet been explored.

352 AC07 describes an algorithm that loops over each observation in serial. Each observation is  
 353 owned by a particular processing element. For each observation  $n$ , the owner of that observa-  
 354 tion broadcasts the observation details (including the observation location, ensemble forward-  
 355 calculated values  $h_n(\mathbf{x}_j)$  for  $j = 1, \dots, N_{\text{ens}}$ , and QC status) to the other processing elements, which  
 356 then each process the observation in parallel. An important innovation of AC07 is the treatment of  
 357 observations themselves as part of the augmented state vector. In other words, just as water vapor,  
 358 temperature, and other geophysical variables are updated by the Kalman filter equations, the ob-  
 359 servations (which are assumed to have a particular location in space) are also updated during the  
 360 assimilation process. Thus the  $n^{\text{th}}$  observation that is broadcast by the owner processing element  
 361 will have been potentially updated by observations 1 through  $n - 1$ . This saves the computational  
 362 expense of having to communicate in order to recompute the observation operators.

363 A scalar form of the ESRF equations (1) is used to efficiently update all of the covariance  
 364 localized state points and observations. The mean of each state  $i$  is updated as

$$\bar{\mathbf{x}}_i = \bar{\mathbf{x}}_i + k_{i,n} \left( \mathbf{y}_n - (\overline{H(\mathbf{X}_f)})_n \right) \quad (28)$$

365 for the Kalman gain  $k_{i,n}$  from equation (2) scalarized for point  $i$  for observation  $n$  as

$$k_{i,n} = \frac{\rho_{i,n}}{d_n} \frac{1}{N_{\text{ens}} - 1} \sum_{j=1}^{N_{\text{ens}}} (\mathbf{X}'_f)_{i,j} (H\mathbf{X})_{n,j}. \quad (29)$$

366 Here,

$$d_n = \frac{1}{N_{\text{ens}} - 1} \sum_{j=1}^{N_{\text{ens}}} (H\mathbf{X})_{n,j}^2 + \mathbf{R}_{n,n}, \quad (30)$$

367 where  $\mathbf{R}_{n,n}$  ( $\mathbf{R}$  is assumed diagonal) is the observation error variance of the  $n^{\text{th}}$  observation, and  
 368  $\rho_{i,n}$  is the localization factor between the state point  $i$  and observation  $n$ , i.e. it corresponds to

369 the  $(i, n)$  component of the  $\rho_{\mathbf{x}, \mathbf{y}}$  matrix in equation (8), although this matrix is not formed in this  
 370 implementation.

371 Similarly, given the scalar square-root correction

$$\beta_n = \frac{1}{1 + \sqrt{r_d}}, \quad (31)$$

372 where

$$r_d = \frac{\mathbf{R}_{n,n}}{d_n}, \quad (32)$$

373 the  $j^{\text{th}}$  ensemble perturbation at state point  $i$  is updated as

$$\mathbf{X}'_{i,j} = \mathbf{X}'_{i,j} + \beta_n k_{i,n} \left( 0 - (\mathbf{H}\mathbf{X})_{n,j} \right). \quad (33)$$

374 Note that the analogous equations are used to update the approximations of the forward observa-  
 375 tion mean  $(\overline{H(\mathbf{X}_f)})_k$  and perturbations  $(\mathbf{H}\mathbf{X})_{k,j}$  for  $k = n + 1$  to  $N_{\text{obs}}$ , i.e. the remaining unassimi-  
 376 lated forward observations are treated as part of the augmented state vector.

## 377 5. Numerical results

378 The implementation described in section 3 was used to replace the computation of  $(\mathbf{E}|\mathbf{g})$  from  
 379 equations (21) and (22) from S17, retaining the remaining components. For comparison, the  
 380 serial method of AC07 was implemented and tested as well. To ensure consistent comparisons, an  
 381 object-oriented approach was incorporated in the Hurricane Ensemble Data Assimilation System  
 382 (HEDAS, Aksoy et al. 2012, 2013; Aksoy 2013; Vukicevic et al. 2013; Aberson et al. 2015) to  
 383 maintain consistency in observation processing, quality control, and disk input/output among all  
 384 three implementations. Only the filter aspect differs.

385 All timings were tested on the NOAA Jet supercomputing system xjet installed in 2015/2016  
 386 where each node has 24 cores with a 2.3 GHz Intel Haswell CPU and 2.66 GB RAM connected  
 387 via FDR Infiniband. As a proof-of-concept for this method, we ran two experiments, each with

388 30 Hurricane WRF (Gopalakrishnan et al. 2010, HWRF) ensemble members, using the Hurri-  
389 cane Edouard (2014) study described in Christophersen et al. (2017). Both of these experiments  
390 use quality-controlled observations from sources including satellite retrievals and the NASA AV6  
391 Global Hawk 20140916GH Storm Survey mission (Zawislak et al. 2016; Rogers et al. 2016;  
392 Christophersen et al. 2017).

393 The first experiment, to illustrate the performance on a relevant single cycle as in Christophersen  
394 et al. (2017), uses HWRF to spin up 30 GFS ensemble members initialized at 2014-09-16 12:00  
395 UTC for 4 hours, then assimilates 15.2K quality-controlled observations from this set at 2014-  
396 09-16 16:00 UTC  $\pm$  30 minutes using the HEDAS system. The localization length-scale was  
397 set to  $L = 240$  as  $c = L/2$  from equation 4.10 of Gaspari and Cohn (1999) as described in S17.  
398 Figure 1 shows the analyzed water vapor field at level 20 (out of 60) for the EPS, MFN, and serial  
399 implementation of AC07. Ten different random observation orderings were assimilated. The mean  
400 and standard deviation of the ten different AC07 analyses are shown in fig. 1a) and 1b). As shown,  
401 the standard deviation of these different orderings can reach up to approximately  $1.5 \text{ g kg}^{-1}$ . The  
402 same 10 random orderings were assimilated with the MFN solution as shown in fig. 1c) and 1d).  
403 Each time, the MFN analysis was identical to within  $10^{-7}$ ; the standard deviation is less than  $10^{-7}$   
404 (“zero”) as well. For comparison, the absolute difference between the average serial analysis and  
405 the EPS analysis is shown in fig. 1e), which as shown is greater than  $2 \text{ g kg}^{-1}$  in places. The  
406 absolute difference between the MFN and EPS solution is shown in fig. 1f), which is also “zero.”

407 To emphasize the order independence issue, figure 2 shows the assimilation of the first two  
408 random observation orderings assimilated in figure 1 (order 1 and order 2). No effort was made to  
409 maximize this difference for AC07 – the first two random orderings were chosen – but likewise no  
410 attempt was made to minimize forecast impact in AC07 by optimizing the ordering as in Kotsuki  
411 et al. (2017). The differences at this level reach up to  $3.5 \text{ g kg}^{-1}$ . The root-mean-squared difference

412 of the entire domain at this level was approximately  $0.5 \text{ g kg}^{-1}$ . However, the MFN analyzed  
413 solutions with different orderings were found to be identical to within  $10^{-8}$ . A similar tolerance  
414 was found by comparing the MFN and EPS solutions.

415 Figure 3a) shows the level 20 water vapor standard deviation (across the ensemble) of the prior  
416 ensemble perturbations  $\mathbf{X}'_f$ , while the standard deviation of the MFN posterior perturbations  $\mathbf{X}'_a$   
417 with orderings 1 and 2 (which are numerically equivalent up to single precision) is shown in fig.  
418 3b). Figure 3c) and 3d) show the standard deviation of  $\mathbf{X}'_a$  at this level for the ordering 1 and 2,  
419 respectively, with the AC07 filter. Figure 3e) shows the two standard deviations differ by up to  
420  $0.1 \text{ g kg}^{-1}$ , while the difference between the AC07 order 1  $\mathbf{X}'_a$  and the EPS solution is up to  $0.35$   
421  $\text{g kg}^{-1}$ . As in the mean, the MFN perturbations and the EPS perturbations are identical to within  
422  $10^{-7}$ .

423 As shown in figures 1 through 3, the differences in the  $\bar{\mathbf{x}}_a$  analysis with random orderings using  
424 the AC07 filter are large enough that they are comparable to the posterior covariance in certain  
425 locations. This is likely due to the highly non-linear nature of the first-cycle tropical cyclone  
426 data assimilation problem. In this application, flights are used as observing platforms to narrow  
427 the inner core uncertainty as shown in figure 3. The first cycle background contains ensemble  
428 members with simulated tropical cyclones with features centered at different locations, leading  
429 to large analysis updates. The main area of uncertainty in the AC07 analyses is actually outside  
430 of the inner core in the south-west quadrant near an area of dry air inflow. As shown, over the  
431 different serial courses of assimilation the order-dependent error standard deviation of this region  
432 can grow to be roughly equivalent in magnitude to the posterior covariance. The matrix function  
433 approach, however, is order independent and therefore removes this source of error and is thus  
434 more numerically consistent with the eigenpair-based solution to the ESRF equations.

435 Having established that in this case the matrix function solution is numerically similar to the  
436 EPS method, which has a proven error bounds, we now turn our attention to the computational  
437 performance of the new method. For this purpose we use a second experimental setup that com-  
438 bines the observations at all times that fall within the same domain as the first experiment. This  
439 leads to up to 35,420 quality-controlled observations that can be used for performance testing.

440 Keeping 1/2 of the total number of observations from all cycles fixed at 17.7K, the scaling as  
441 a function of number of cores is shown in figure 4. The matrix function method scales nearly  
442 linearly as a function of the number of processing elements as in S17, but overall the wall time  
443 remains bound by I/O time.

444 As a function of the number of observations the MFN implementation scales much better than  
445 the eigenproblem-based solution (EPS) as shown in figure 5, where the number of processing  
446 elements is fixed at 386,  $L = 240$  for the correlation length-scale, and the number of observations  
447 vary. As discussed in S17,  $L = 240$  leads to points across more than half of the domain being  
448 correlated which in turn leads to a relatively dense, nearly full-rank matrix. As predicted by theory,  
449 the EPS solution appears to scale as the cube of the number of observations. However, the MFN  
450 approach apparently scales linearly. Times for the EPS solution longer than 45 minutes are not  
451 shown. With 17.7k observations on 386 processing elements, the EPS solution took 41 minutes  
452 and 28 seconds to complete from start to finish (including expensive disk reading and writing),  
453 while the MFN solution took only 16 minutes and 42 seconds. The MFN solution continues to  
454 scale well even at 35.4K observations, completing in 30 minutes and 45 seconds, which is still  
455 more than 10 minutes faster than the EPS solution with half as many observations. Therefore, as  
456 shown, the MFN approach scales much better as function of the number of observations than the  
457 EPS solution.

458 The MFN solution is also roughly comparable to the AC07 solution in terms of wall time. While  
459 the MFN approach is actually slightly faster for small amounts of observations, for the largest  
460 number of observations tested (35.4K observations) the serial filter is faster with a wall time of 28  
461 minutes 24 seconds as opposed to 30 minutes 45 seconds. However, the wall-time differences are  
462 small enough that the observation order independence of MFN apparently makes it competitive  
463 with AC07 for these numbers of observations. This is somewhat surprising as the only communi-  
464 cation used by the AC07 filter is to broadcast observations, while distributed matrix multiplications  
465 are required by the MFN approach. However, the MFN approach has the potential benefit that it  
466 does not serially iterate over the observations, but instead can process all observations in parallel.

467 The number of matrix multiplications, and hence the overall timing of the matrix function solu-  
468 tion, is directly related to the number of restarts and  $m$ , the maximum basis size before restarting.  
469 Increasing  $m$  leads to fewer restarts but requires additional memory and dense matrix processing  
470 time. The number of Eiermann-Ernst restarts necessary for convergence with  $m = 150$  as used  
471 in our study ranged from 1 for the smallest number of observations (2,760) to 2 for the largest  
472 number of observations (35,420). The SLEPc error estimate at the end of each restart iteration for  
473 the smallest number of observations was on the order of  $10^{-2}$  for  $k = 0$  and  $10^{-15}$  for  $k = 1$ , while  
474 for the largest the error was on the order of  $10^{-2}$  for  $k = 0$ ,  $10^{-8}$  for  $k = 1$ , and  $10^{-13}$  for  $k = 2$ . It  
475 appears the number of restarts grows very weakly with  $N_{\text{obs}}$ .

476 Table 1 shows the time necessary to solve the matrix function portion of the ESRF equations  
477 per ensemble member with  $L = 240$  for the 17.7k observation case as a function of varying the  $m$   
478 parameter. As shown,  $m$  less than 100 requires an excessive amount of restarts and total matrix  
479 product evaluations; for  $m$  greater than 100, the overall performance is dependent upon the exact  
480 number of matrix product evaluations required to reach the numerical accuracy of  $\epsilon_{\text{tol}} = 10^{-8}$ .  
481 For this case,  $m = 125$  requires the fewest number of matrix-product evaluations, which is highly



482 correlated with the total amount of MFN solve time. Table 2 shows the same results with the  
483 localization length-scale  $L = 60$ . In this case,  $m = 150$  gives the optimal results. The best particular  
484 value of  $m$  therefore depends upon the factorization of the total number of evaluations required.  $m$   
485 larger than 100 is recommended to avoid excessive restarting, and  $m$  less than 200 is recommended  
486 due to the expense of dense matrix evaluations. We choose  $m = 150$  to split the difference.

487 The scaling of memory usage on 386 xjet processors as a function of number of observations  
488 is shown in fig. 6. As shown, and as expected by theory, the EPS solution memory usage scales  
489 cubically as a function of the number of observations. The serial filter of AC07 apparently scales  
490 linearly as it only processes a single observation at once. The MFN solution, which currently  
491 stores the entire sparse  $\mathbf{C}_{H_x, H_x}$  matrix in memory, scales better than S17 but apparently worse than  
492 linearly. This is because with  $L = 240$  the  $\mathbf{C}_{H_x, H_x}$  matrix is relatively dense. For a dense matrix,  
493 the memory requirements would be quadratic, while for a sparse matrix the memory requirements  
494 would be closer to linear. The memory scaling here is consistent with a factor somewhere in  
495 between quadratic and linear. Note, however, that the expense here is related to the representation  
496 of  $\mathbf{C}_{H_x, H_x}$  and not directly to the MFN approach.

497 Indeed, the computational performance of the MFN method comes down to computing the ma-  
498 trix product. As mentioned, as only  $\mathbf{D}\mathbf{b}$  is required in this method, it is not necessary to explicitly  
499 store the matrix  $\mathbf{D}$  in memory. This so-called “matrix-free method” was implemented and tested  
500 successfully. As a first test, we used a simple implementation that brute-force recalculated the ele-  
501 ments of  $\mathbf{C}_{H_x, H_x}$  when required and avoided storing these elements in memory. While the memory  
502 usage decreased as expected, the time necessary to recompute the covariances made the method  
503 uncompetitive with the stored-in-memory matrix approach. The matrix-free implementation took  
504 29:19 minutes on 386 processors for 4.5k observations versus just 5:40 minutes with a stored ma-

505 trix. A more suitable matrix-free implementation such one based on FFT would make this feature  
506 of the matrix function algorithm more attractive. Additional research is required in this area.

507 As an additional note, the MFN approach for solving the mean  $\mathbf{x} = f_1(\mathbf{D})(\mathbf{y} - \overline{H(\mathbf{X}_f)})$  was  
508 compared with the more traditional method of solving for  $\mathbf{D}\mathbf{x} = \mathbf{y} - \overline{H(\mathbf{X}_f)}$  using GMRES. In  
509 this particular case, the MFN was found to be competitive with GMRES. This may be due to  
510 the fact that  $\mathbf{D}$  is relatively dense and an efficient pre-conditioner for use with GMRES was not  
511 found. Regardless, the novel contribution here is computing the more difficult  $f_2(\mathbf{D})(\mathbf{0} - H\mathbf{X})$   
512 using MFN.

## 513 **6. Discussion and conclusions**

514 In this work we describe the utilization of matrix functions, a powerful linear algebra tool, to  
515 derive numerically accurate and efficient solutions of the ESRF equations. With this method, high-  
516 rank localized covariance matrices can be applied consistently in such a way that the final analysis  
517 does not depend upon the ordering of observations. For the number of observations investigated,  
518 this method is roughly competitive in terms of wall-time with the highly efficient serial filter of  
519 AC07.

520 The matrix function approach is built on the Arnoldi iteration, which provides a basis for the  
521 Krylov subspace spanned by the covariance matrix of the forward-computed observations  $\mathbf{C}_{H\mathbf{x},H\mathbf{x}}$   
522 and a vector  $\mathbf{b}$ . This basis allows for evaluation of the ESRF matrix functions over a much smaller,  
523 upper Hessenberg matrix. The Scalable Library for Eigenproblem Computation (SLEPc, Her-  
524 nandez et al. 2005) includes an efficient implementation of the matrix function method along with  
525 the Eiermann-Ernst restart (Eiermann and Ernst 2006). Only the matrix-vector product is required,  
526 which can be used to provide matrix-free implementations, although for performance reasons stor-  
527 ing the entire sparse  $\mathbf{C}_{H\mathbf{x},H\mathbf{x}}$  matrix across processing elements may be preferable as shown in our

528 case. The ability to consistently incorporate high-rank covariance models with a known error  
529 bounds provides a platform to investigate hybrid ensemble/climatological covariances as well as  
530 observation versus model space covariance issues.

531 Additional effort will be needed to fully understand the computational performance of this  
532 method in comparison to other existing parallel EnKF techniques, but a few basic conclusions can  
533 be drawn. First, in comparison to the S17 eigenpair solution method of Steward et al. (2017), the  
534 matrix function approach scales much better as a function of the number of observations assimilated  
535 and uses less memory while maintaining independence of observation ordering and achieving  
536 nearly identical numerical results. Second, while this method and the Consistent Hybrid Ensemble  
537 Filter of Bishop et al. (2015, CHEF) are similarly independent of the order of observations for  
538 high-rank covariance models, as the matrix function approach applies the high-rank covariance  
539 matrices globally, it may be more computationally efficient than CHEF (which applies the matrices  
540 locally), especially for long localization lengths. This approach also solves the ESRF equations  
541 rather using than perturbed observations. Finally, the matrix function method is competitive with  
542 the serial AC07 implementation of Anderson and Collins (2007) in terms of wall-time for the cases  
543 tested here. While it uses more memory, the matrix function approach is shown to be more faithful  
544 to the eigenpair-based solution of the ESRF equations than AC07. It is unknown if this additional  
545 precision will have a positive impact on forecasts. The recent work of Emanuel and Zhang (2017)  
546 demonstrates the crucial impact of inner core moisture on TC predictability, and the two serial  
547 AC07 analyses shown in fig. 2 with merely different observation orderings differ on the extent of  
548 dry air near the inner core. As shown, the two water vapor analyses for this difficult first-cycle TC  
549 case can differ by up to  $3 \text{ g kg}^{-1}$ , and therefore it is reasonable to expect the two serial analyses  
550 shown in figure 2 may produce qualitatively different medium-term forecasts. A method that can  
551 increase fidelity to the ESRF equations, known to be the minimum variance solution (e.g. Bishop

552 et al. 2015), for tropical cyclone cases may be worth the additional computational expense. Due to  
553 the efficiency and ease of implementation of the serial filter, continued research into minimizing  
554 observation ordering impact is also likely to be beneficial.

555 Comparison of this method to other local analysis methods remains more unclear. The perfor-  
556 mance of local analysis methods is most critically related to the radius of influence. For large  
557 radii as considered here, this would likely make local analysis methods inefficient as the problem  
558 for each local grid point becomes nearly as large as the entire domain. However, in such cases,  
559 when sample-based covariance localization is utilized with the ESRF approach, the matrix func-  
560 tion approach could also potentially be used to improve performance versus  $O(n^3)$  algorithms such  
561 as finding eigenpairs or the Cholesky decomposition. This may be unnecessary, however, if the  
562 number of local observations does not exceed  $\approx 10^2$ .

563 At the moment, a major weakness of the non-local matrix function approach in comparison to  
564 the AC07 serial approach is the memory usage scaling. Extrapolating the results presented in  
565 figure 6 on 386 processors and keeping the number of processors constant, with approximately  
566 80k observations (assuming quadratic growth) to 115k observations (assuming linear growth) the  
567 matrix function approach would run out of memory. By comparison, the serial filter would run  
568 out of memory (assuming linear growth) at approximately 3.2 million observations. A matrix free  
569 implementation would address this issue. Since in the matrix function approach, computational  
570 performance comes down efficient methods of applying the matrix product, we aim to investigate  
571 application of the modulation product of Bishop and Hodyss (2009) to apply correlations in or-  
572 der improve the memory scaling issue. In the meantime, batch processing of large numbers of  
573 observations is one potential work-around.

574 The algorithm described in this paper requires a distributed sparse matrix implementation such  
575 as that available in the Portable Extensible Toolkit for Scientific Computing (PETSc, Balay et al.

576 1997, 2016, 2017) which SLEPc is built upon. In addition, the restarted Arnoldi process (including  
577 a numerically stable parallel Gram-Schmidt orthogonalization process) must be implemented to  
578 estimate the required reduced-order matrix function products. When using the SLEPc library that  
579 provides this functionality, this approach is not more difficult than the eigenpair implementation  
580 of S17. However, either implementation is certainly more complex than the serial approximation.

581 Finally, while the order-dependency issue shown here is non-trivial, the TC first-cycle case is  
582 likely to be a “worst-case” scenario due to the highly non-linear nature of feature misalignment.  
583 While Nerger (2015) hypothesized that the effect of the observation-order dependency in the serial  
584 implementation is small when the analysis is not far from the prior, the filter described here may be  
585 useful to test the practical effect of this hypothesis in a variety of large-scale cases and to develop  
586 mitigation solutions for the serial approach when necessary.

587 *Acknowledgments.* This research was partially funded by the NOAA Hurricane Forecast Im-  
588 provement Project award number NA14NWS4680022. This work was partially supported by  
589 Agencia Estatal de Investigación (AEI) under grant TIN2016-75985-P, which includes European  
590 Commission ERDF funds. Alejandro Lamas Daviña was supported by the Spanish Ministry of  
591 Education, Culture and Sport through a grant with reference FPU13-06655. The fourth author’s  
592 work was in part carried out under the auspices of CIMAS, a joint institute of the University  
593 of Miami and NOAA, cooperative agreement NA15OAR4320064. The authors acknowledge the  
594 NOAA Research and Development High Performance Computing Program for providing comput-  
595 ing and storage resources that have contributed to the research results reported within this paper.  
596 URL: <http://rdhpcs.noaa.gov>. We thank Jeff Anderson, Shu-Chih Yang, and three anony-  
597 mous reviewers for their helpful comments and contributions. We also thank Hui Christophersen  
598 for providing technical assistance.

599 **References**

- 600 Aberson, S. D., A. Aksoy, K. J. Sellwood, T. Vukicevic, and X. Zhang, 2015: Assimilation  
601 of High-Resolution Tropical Cyclone Observations with an Ensemble Kalman Filter Using  
602 HEDAS: Evaluation of 2008–11 HWRF Forecasts. *Monthly Weather Review*, **143** (2), 511–523,  
603 doi:10.1175/MWR-D-14-00138.1.
- 604 Afanasjew, M., M. Eiermann, O. G. Ernst, and S. Güttel, 2008: Implementation of a restarted  
605 Krylov subspace method for the evaluation of matrix functions. *Linear Algebra and its Appli-*  
606 *cations*, **429** (10), 2293–2314, doi:10.1016/j.laa.2008.06.029.
- 607 Aksoy, A., 2013: Storm-Relative Observations in Tropical Cyclone Data Assimilation with  
608 an Ensemble Kalman Filter. *Monthly Weather Review*, **141** (2), 506–522, doi:10.1175/  
609 MWR-D-12-00094.1.
- 610 Aksoy, A., S. D. Aberson, T. Vukicevic, K. J. Sellwood, S. Lorsolo, and X. Zhang, 2013: Assimi-  
611 lation of High-Resolution Tropical Cyclone Observations with an Ensemble Kalman Filter Using  
612 NOAA/AOML/HRD’s HEDAS: Evaluation of the 2008–11 Vortex-Scale Analyses. *Monthly*  
613 *Weather Review*, **141** (6), 1842–1865, doi:10.1175/MWR-D-12-00194.1.
- 614 Aksoy, A., S. Lorsolo, T. Vukicevic, K. J. Sellwood, S. D. Aberson, and F. Zhang, 2012: The  
615 HWRF Hurricane Ensemble Data Assimilation System (HEDAS) for High-Resolution Data:  
616 The Impact of Airborne Doppler Radar Observations in an OSSE. *Monthly Weather Review*,  
617 **140** (6), 1843–1862.
- 618 Anderson, J. L., 2001: An Ensemble Adjustment Kalman Filter for Data Assimilation. *Monthly*  
619 *Weather Review*, **129**, 2884–2903, doi:10.1175/1520-0493(2001)129<2884:AEAKFF>2.0.CO;  
620 2.

621 Anderson, J. L., 2003: A Local Least Squares Framework for Ensemble Filtering. *Monthly*  
622 *Weather Review*, **131** (4), 634–642, doi:10.1175/1520-0493(2003)131<0634:ALLSFF>2.0.CO;  
623 2.

624 Anderson, J. L., 2012: Localization and Sampling Error Correction in Ensemble Kalman  
625 Filter Data Assimilation. *Monthly Weather Review*, **140** (7), 2359–2371, doi:10.1175/  
626 MWR-D-11-00013.1.

627 Anderson, J. L., and N. Collins, 2007: Scalable Implementations of Ensemble Filter Algorithms  
628 for Data Assimilation. *Journal of Atmospheric and Oceanic Technology*, **24** (8), 1452–1463,  
629 doi:10.1175/JTECH2049.1.

630 Arnoldi, W. E., 1951: The principle of minimized iterations in the solution of the matrix eigenvalue  
631 problem. *Quarterly of Applied Mathematics*, **9** (1), 17–29, doi:10.1090/qam/42792.

632 Balay, S., W. D. Gropp, L. C. McInnes, and B. F. Smith, 1997: Efficient management of parallelism  
633 in object-oriented numerical software libraries. *Modern software tools for scientific computing*,  
634 Springer, 163–202.

635 Balay, S., and Coauthors, 2016: PETSc Users Manual. Tech. Rep. ANL-95/11 - Revision 3.7,  
636 Technical report, Argonne National Laboratory (ANL). URL [http://www.mcs.anl.gov/petsc/  
637 petsc-current/docs/manual.pdf](http://www.mcs.anl.gov/petsc/petsc-current/docs/manual.pdf).

638 Balay, S., and Coauthors, 2017: PETSc: Home Page. URL <https://www.mcs.anl.gov/petsc/>.

639 Bessho, K., and Coauthors, 2016: An Introduction to Himawari-8/9 — Japan’s New-Generation  
640 Geostationary Meteorological Satellites. *Journal of the Meteorological Society of Japan. Ser. II*,  
641 **94** (2), 151–183, doi:10.2151/jmsj.2016-009.

- 642 Bishop, C. H., B. J. Etherton, and S. J. Majumdar, 2001: Adaptive sampling with the ensemble  
643 transform Kalman filter. Part I: Theoretical aspects. *Monthly Weather Review*, **129** (3), 420–436.
- 644 Bishop, C. H., and D. Hodyss, 2009: Ensemble covariances adaptively localized with ECO-RAP.  
645 Part 2: a strategy for the atmosphere. *Tellus A*, **61** (1), 97–111, doi:10.1111/j.1600-0870.2008.  
646 00372.x.
- 647 Bishop, C. H., B. Huang, and X. Wang, 2015: A Nonvariational Consistent Hybrid Ensemble  
648 Filter. *Monthly Weather Review*, **143** (12), 5073–5090, doi:10.1175/MWR-D-14-00391.1.
- 649 Björck, Å., 1994: Numerics of Gram-Schmidt orthogonalization. *Linear Algebra and its Applica-*  
650 *tions*, **197-198 (Supplement C)**, 297–316, doi:10.1016/0024-3795(94)90493-6.
- 651 Burgers, G., P. J. van Leeuwen, and G. Evensen, 1998: Analysis scheme in the ensemble Kalman  
652 filter. *Monthly Weather Review*, **126** (6), 1719–1724.
- 653 Campbell, W. F., C. H. Bishop, and D. Hodyss, 2010: Vertical Covariance Localization for Satellite  
654 Radiances in Ensemble Kalman Filters. *Monthly Weather Review*, **138** (1), 282–290, doi:10.  
655 1175/2009MWR3017.1.
- 656 Chang, C.-C., S.-C. Yang, and C. Keppenne, 2014: Applications of the Mean Recentering Scheme  
657 to Improve Typhoon Track Prediction: A Case Study of Typhoon Nanmadol (2011). *Journal of*  
658 *the Meteorological Society of Japan. Ser. II*, **92** (6), 559–584, doi:10.2151/jmsj.2014-604.
- 659 Christophersen, H., A. Aksoy, J. Dunion, and K. Sellwood, 2017: The Impact of NASA  
660 Global Hawk Unmanned Aircraft Dropwindsonde Observations on Tropical Cyclone Track,  
661 Intensity, and Structure: Case Studies. *Monthly Weather Review*, **145** (5), 1817–1830, doi:  
662 10.1175/MWR-D-16-0332.1.



663 Deadman, E., N. J. Higham, and R. Ralha, 2012: Blocked Schur Algorithms for Computing the  
664 Matrix Square Root. *Applied Parallel and Scientific Computing*, Springer, Berlin, Heidelberg,  
665 171–182, Lecture Notes in Computer Science, doi:10.1007/978-3-642-36803-5\_12.

666 Eiermann, M., and O. Ernst, 2006: A Restarted Krylov Subspace Method for the Evaluation  
667 of Matrix Functions. *SIAM Journal on Numerical Analysis*, **44** (6), 2481–2504, doi:10.1137/  
668 050633846.

669 Eiermann, M., O. Ernst, and S. Güttel, 2011: Deflated Restarting for Matrix Functions. *SIAM*  
670 *Journal on Matrix Analysis and Applications*, **32** (2), 621–641, doi:10.1137/090774665.

671 Emanuel, K., and F. Zhang, 2017: The Role of Inner-Core Moisture in Tropical Cyclone Pre-  
672 dictability and Practical Forecast Skill. *Journal of the Atmospheric Sciences*, **74** (7), 2315–2324,  
673 doi:10.1175/JAS-D-17-0008.1.

674 Evensen, G., 1994: Sequential data assimilation with a nonlinear quasi-geostrophic model using  
675 Monte Carlo methods to forecast error statistics. *Journal of Geophysical Research*, **99** (10),  
676 143–10, doi:/doi/10.1029/94JC00572.

677 Frayssé, V., L. Giraud, and H. Kharraz-Aroussi, 1998: On the influence of the orthogonalization  
678 scheme on the parallel performance of GMRES. *Euro-Par'98 Parallel Processing*, Springer,  
679 Berlin, Heidelberg, 751–762, Lecture Notes in Computer Science, doi:10.1007/BFb0057927.

680 Frommer, A., K. Lund, M. Schweitzer, and D. Szyld, 2017: The Radau–Lanczos Method for  
681 Matrix Functions. *SIAM Journal on Matrix Analysis and Applications*, 710–732, doi:10.1137/  
682 16M1072565.

- 683 Gaspari, G., and S. E. Cohn, 1999: Construction of correlation functions in two and three di-  
684 mensions. *Quarterly Journal of the Royal Meteorological Society*, **125 (554)**, 723–757, doi:  
685 10.1002/qj.49712555417.
- 686 Godinez, H. C., and J. D. Moulton, 2012: An efficient matrix-free algorithm for the ensemble  
687 Kalman filter. *Computational Geosciences*, **16 (3)**, 565–575, doi:10.1007/s10596-011-9268-9.
- 688 Golub, G. H., and C. F. Van Loan, 1996: *Matrix computations*, Vol. 3. Johns Hopkins University  
689 Press.
- 690 Gopalakrishnan, S. G., F. Marks, X. Zhang, J.-W. Bao, K.-S. Yeh, and R. Atlas, 2010: The Ex-  
691 perimental HWRF System: A Study on the Influence of Horizontal Resolution on the Structure  
692 and Intensity Changes in Tropical Cyclones Using an Idealized Framework. *Monthly Weather*  
693 *Review*, **139 (6)**, 1762–1784, doi:10.1175/2010MWR3535.1.
- 694 Hamill, T. M., J. S. Whitaker, and C. Snyder, 2001: Distance-Dependent Filtering of Background  
695 Error Covariance Estimates in an Ensemble Kalman Filter. *Monthly Weather Review*, **129 (11)**,  
696 2776–2790, doi:10.1175/1520-0493(2001)129<2776:DDFOBE>2.0.CO;2.
- 697 Hernandez, V., J. E. Roman, and A. Tomas, 2007: Parallel Arnoldi eigensolvers with enhanced  
698 scalability via global communications rearrangement. *Parallel Computing*, **33 (7)**, 521–540,  
699 doi:10.1016/j.parco.2007.04.004.
- 700 Hernandez, V., J. E. Roman, and V. Vidal, 2005: SLEPc: A Scalable and Flexible Toolkit for  
701 the Solution of Eigenvalue Problems. *ACM Transactions on Mathematical Software*, **31 (3)**,  
702 351–362, doi:10.1145/1089014.1089019.
- 703 Higham, N., 2008: *Functions of Matrices*. Other Titles in Applied Mathematics, Society for In-  
704 dustrial and Applied Mathematics.

- 705 Higham, N. J., 1987: Computing real square roots of a real matrix. *Linear Algebra and its Appli-*  
706 *cations*, **88**, 405–430, doi:10.1016/0024-3795(87)90118-2.
- 707 Hochbruck, M., and C. Lubich, 1997: On Krylov Subspace Approximations to the Matrix Ex-  
708 ponential Operator. *SIAM Journal on Numerical Analysis*, **34 (5)**, 1911–1925, doi:10.1137/  
709 S0036142995280572.
- 710 Houtekamer, P. L., B. He, and H. L. Mitchell, 2013: Parallel Implementation of an Ensemble  
711 Kalman Filter. *Monthly Weather Review*, **142 (3)**, 1163–1182, doi:10.1175/MWR-D-13-00011.  
712 1.
- 713 Houtekamer, P. L., and H. L. Mitchell, 1998: Data assimilation using an ensemble Kalman filter  
714 technique. *Monthly Weather Review*, **126 (3)**, 796–811.
- 715 Houtekamer, P. L., and H. L. Mitchell, 2001: A Sequential Ensemble Kalman Filter for  
716 Atmospheric Data Assimilation. *Monthly Weather Review*, **129 (1)**, 123–137, doi:10.1175/  
717 1520-0493(2001)129(0123:ASEKFF)2.0.CO;2.
- 718 Hunt, B. R., E. J. Kostelich, and I. Szunyogh, 2007: Efficient data assimilation for spatiotemporal  
719 chaos: A local ensemble transform Kalman filter. *Physica D: Nonlinear Phenomena*, **230 (1-2)**,  
720 112–126.
- 721 Kalman, R. E., 1960: A new approach to linear filtering and prediction problems. *Journal of Basic*  
722 *Engineering*, **82 (1)**, 35–45.
- 723 Keppenne, C. L., and M. M. Rienecker, 2002: Initial Testing of a Massively Parallel Ensemble  
724 Kalman Filter with the Poseidon Isopycnal Ocean General Circulation Model. *Monthly Weather*  
725 *Review*, **130 (12)**, 2951–2965, doi:10.1175/1520-0493(2002)130(2951:ITOAMP)2.0.CO;2.

- 726 Kotsuki, S., S. J. Greybush, and T. Miyoshi, 2017: Can We Optimize the Assimilation Order in the  
727 Serial Ensemble Kalman Filter? A Study with the Lorenz-96 Model. *Monthly Weather Review*,  
728 **145 (12)**, 4977–4995, doi:10.1175/MWR-D-17-0094.1.
- 729 Miyoshi, T., and Coauthors, 2016: “Big Data Assimilation” – Revolutionizing Severe Weather  
730 Prediction. *Bulletin of the American Meteorological Society*, **97 (8)**, 1347–1354, doi:10.1175/  
731 BAMS-D-15-00144.1.
- 732 Nerger, L., 2015: On Serial Observation Processing in Localized Ensemble Kalman Filters.  
733 *Monthly Weather Review*, **143 (5)**, 1554–1567, doi:10.1175/MWR-D-14-00182.1.
- 734 Nino-Ruiz, E. D., A. Sandu, and J. Anderson, 2015: An efficient implementation of the ensem-  
735 ble Kalman filter based on an iterative Sherman–Morrison formula. *Statistics and Computing*,  
736 **25 (3)**, 561–577, doi:10.1007/s11222-014-9454-4.
- 737 Nino-Ruiz, E. D., A. Sandu, and X. Deng, 2017: A parallel implementation of the ensemble  
738 Kalman filter based on modified Cholesky decomposition. *Journal of Computational Science*,  
739 doi:10.1016/j.jocs.2017.04.005.
- 740 Ott, E., and Coauthors, 2002: A Local Ensemble Kalman Filter for Atmospheric Data Assimila-  
741 tion. *arXiv:physics/0203058*, arXiv: physics/0203058.
- 742 Rogers, R. F., J. A. Zhang, J. Zawislak, H. Jiang, G. R. Alvey, E. J. Zipser, and S. N. Stevenson,  
743 2016: Observations of the Structure and Evolution of Hurricane Edouard (2014) during Intensity  
744 Change. Part II: Kinematic Structure and the Distribution of Deep Convection. *Monthly Weather*  
745 *Review*, **144 (9)**, 3355–3376, doi:10.1175/MWR-D-16-0017.1.
- 746 Saad, Y., 1992: Analysis of Some Krylov Subspace Approximations to the Matrix Exponential  
747 Operator. *SIAM Journal on Numerical Analysis*, **29 (1)**, 209–228, doi:10.1137/0729014.

- 748 Sakov, P., and L. Bertino, 2011: Relation between two common localisation methods for the EnKF.  
749 *Computational Geosciences*, **15** (2), 225–237, doi:10.1007/s10596-010-9202-6.
- 750 Schmit, T. J., P. Griffith, M. M. Gunshor, J. M. Daniels, S. J. Goodman, and W. J. Lehair, 2016:  
751 A Closer Look at the ABI on the GOES-R Series. *Bulletin of the American Meteorological*  
752 *Society*, **98** (4), 681–698, doi:10.1175/BAMS-D-15-00230.1.
- 753 Steward, J. L., A. Aksoy, and Z. S. Haddad, 2017: Parallel Direct Solution of the Ensemble Square  
754 Root Kalman Filter Equations with Observation Principal Components. *Journal of Atmospheric*  
755 *and Oceanic Technology*, **34** (9), 1867–1884, doi:10.1175/JTECH-D-16-0140.1.
- 756 Tippett, M. K., J. L. Anderson, C. H. Bishop, T. M. Hamill, and J. S. Whitaker, 2003: En-  
757 semble Square Root Filters. *Monthly Weather Review*, **131** (7), 1485–1490, doi:10.1175/  
758 1520-0493(2003)131<1485:ESRF>2.0.CO;2.
- 759 Van Der Vorst, H. A., 1987: An iterative solution method for solving  $f(A)x = b$ , using Krylov  
760 subspace information obtained for the symmetric positive definite matrix  $A$ . *Journal of Compu-*  
761 *tational and Applied Mathematics*, **18** (2), 249–263, doi:10.1016/0377-0427(87)90020-3.
- 762 Vukicevic, T., A. Aksoy, P. Reasor, S. D. Aberson, K. J. Sellwood, and F. Marks, 2013: Joint Im-  
763 pact of Forecast Tendency and State Error Biases in Ensemble Kalman Filter Data Assimilation  
764 of Inner-Core Tropical Cyclone Observations. *Monthly Weather Review*, **141** (9), 2992–3006,  
765 doi:10.1175/MWR-D-12-00211.1.
- 766 Wang, Y., Y. Jung, T. A. Supinie, and M. Xue, 2013: A Hybrid MPI–OpenMP Parallel Al-  
767 gorithm and Performance Analysis for an Ensemble Square Root Filter Designed for Multi-  
768 scale Observations. *Journal of Atmospheric and Oceanic Technology*, **30** (7), 1382–1397, doi:  
769 10.1175/JTECH-D-12-00165.1.

- 770 Whitaker, J. S., and T. M. Hamill, 2002: Ensemble Data Assimilation without Perturbed Observa-  
771 tions. *Monthly Weather Review*, **130** (7), 1913–1924, doi:10.1175/1520-0493(2002)130<1913:  
772 EDAWPO>2.0.CO;2.
- 773 Zawislak, J., H. Jiang, G. R. Alvey, E. J. Zipser, R. F. Rogers, J. A. Zhang, and S. N. Stevenson,  
774 2016: Observations of the Structure and Evolution of Hurricane Edouard (2014) during Intensity  
775 Change. Part I: Relationship between the Thermodynamic Structure and Precipitation. *Monthly*  
776 *Weather Review*, **144** (9), 3333–3354, doi:10.1175/MWR-D-16-0018.1.
- 777 Zhang, S., M. J. Harrison, A. T. Wittenberg, A. Rosati, J. L. Anderson, and V. Balaji, 2005: Ini-  
778 tialization of an ENSO Forecast System Using a Parallelized Ensemble Filter. *Monthly Weather*  
779 *Review*, **133** (11), 3176–3201, doi:10.1175/MWR3024.1.

780 **LIST OF TABLES**

781 **Table 1.** Time to complete the solution, number of restarts (per control vector), and to-  
782 tal number of matrix product evaluations as a function of  $m$ , the size of the  
783 Krylov subspace before restarting, required to solve the perturbation update  
784 matrix function  $f_2$  in equation (24) with  $L = 240$  (in equations (5) and (8)) and  
785 17.7K observations as described in section 5. The timings are with a single MPI  
786 process on an Intel Core i7 server. Note these times are for a single ensemble  
787 member. . . . . 39

788 **Table 2.** As in table 1 but with  $L = 60$ . The reduction in time versus  $L = 240$  is due to  
789 the increased sparsity of the localization matrices  $\rho_{y,y}$  and  $\rho_{x,y}$ . . . . . 40

790 TABLE 1. Time to complete the solution, number of restarts (per control vector), and total number of matrix  
791 product evaluations as a function of  $m$ , the size of the Krylov subspace before restarting, required to solve  
792 the perturbation update matrix function  $f_2$  in equation (24) with  $L = 240$  (in equations (5) and (8)) and 17.7K  
793 observations as described in section 5. The timings are with a single MPI process on an Intel Core i7 server.  
794 Note these times are for a single ensemble member.

$m$	Time (s)	Restarts	Total evals
25	2.5743e+04	74	1875
50	4.8219e+03	12.2	660
75	3.2298e+03	5	450
100	2.8686e+03	3	400
125	2.6897e+03	2	375
150	3.2460e+03	2	450
175	2.5257e+03	1	350
200	2.8950e+03	1	400



795 TABLE 2. As in table 1 but with  $L = 60$ . The reduction in time versus  $L = 240$  is due to the increased sparsity  
 796 of the localization matrices  $\rho_{y,y}$  and  $\rho_{x,y}$ .

$m$	Time (s)	Restarts	Total evals
25	1.6822e+04	66.2	1705
50	3.8763e+03	15.0333	802
75	2.7369e+03	6.9	593
100	2.2974e+03	4	500
125	2.2872e+03	3	500
150	2.0749e+03	2	450
175	2.4319e+03	2	525
200	2.2491e+03	1.43333	487

797 **LIST OF FIGURES**

798 **Fig. 1.** Comparison between water vapor ( $\text{g kg}^{-1}$ ) at level 20 (of 60 total, corresponding to a height  
 799 of approximately 2.5 km) of the Hurricane Edouard single cycle case of Christophersen et al.  
 800 (2017) with 15.2K observations and  $L = 240$  as described in S17. Ten different random  
 801 orderings of observations were used. (a) The average of the ten AC07  $\bar{x}_a$  analyses. (b) The  
 802 standard deviation of these ten AC07  $\bar{x}_a$  analyses. (c) The average of the ten matrix function  
 803 (MFN)  $\bar{x}_a$  analyses. (d) The standard deviation of the MFN analyses, which is less than  
 804  $10^{-7}$  at all points. (e) The absolute difference between (a) and the EPS solution. (f) The  
 805 absolute difference between (c) and the EPS solution (also less than  $10^{-7}$  for all points). . . . 42

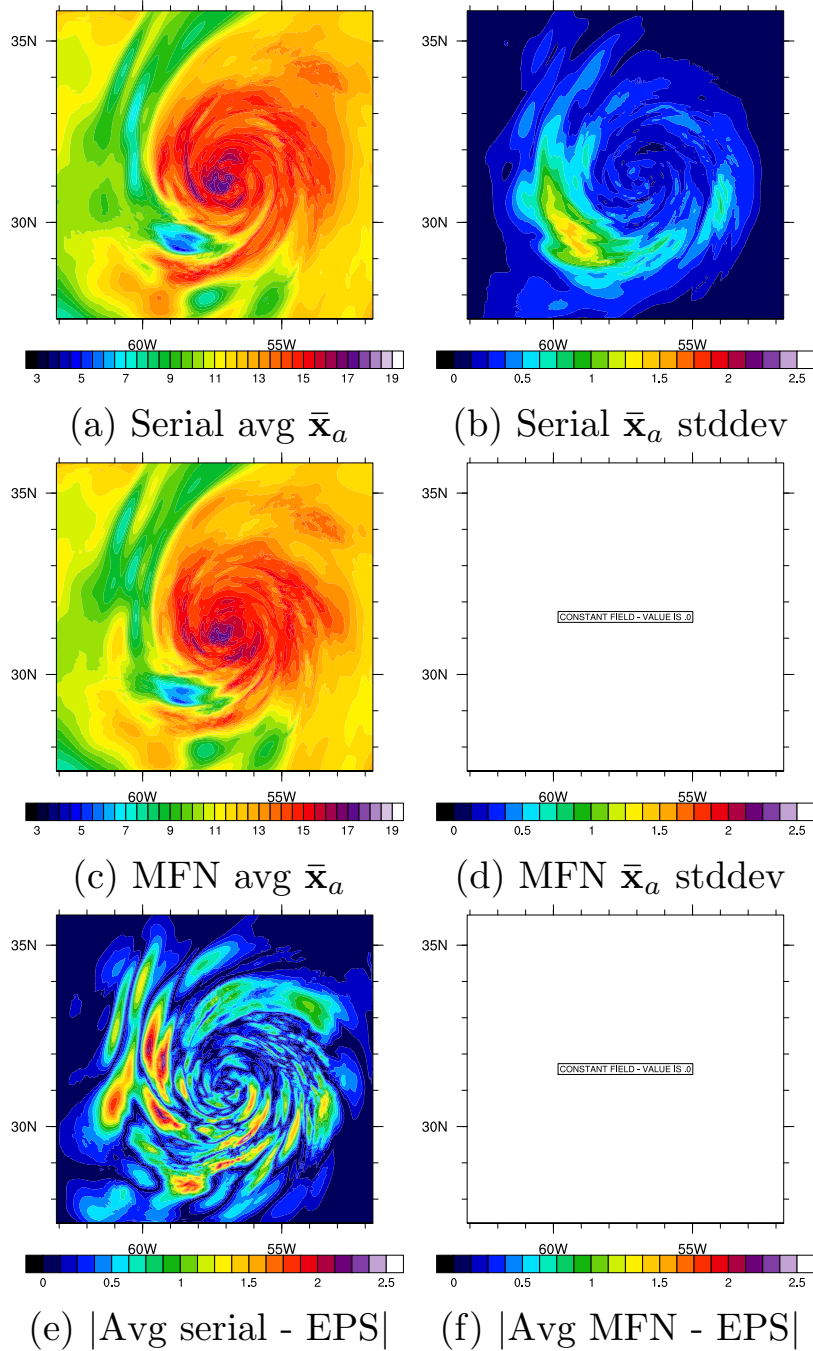
806 **Fig. 2.** Comparison between analyzed  $\bar{x}_a$  level 20 water vapor as in fig. 1 for two of the ten different  
 807 random orderings of observations. (a) The serial filter of Anderson and Collins (2007) with  
 808 ordering 1 and (b) ordering 2. (c) MFN analyzed  $\bar{x}_a$  ordering 1. (d) MFN  $\bar{x}_a$  ordering 2. (e)  
 809 The absolute value difference between (a) and (b). (f) The difference between the two MFN  
 810 orderings in (c) and (d), which is less than  $10^{-7}$ . The difference between the MFN and EPS  
 811 analysis for this case is also less than  $10^{-7}$  at all levels. . . . . 43

812 **Fig. 3.** Ensemble spread (i.e. standard deviations over the ensemble) of water vapor ( $\text{g kg}^{-1}$ ) at level  
 813 20 as in figures 1 and 2. Here the first two random orderings of observations were used as in  
 814 fig. 2. (a) The standard deviation of the prior distribution  $\mathbf{X}'_f$  at this level. (b) The standard  
 815 deviation of the MFN posterior distribution  $\mathbf{X}'_a$  (ordering 1, 2, and the EPS solution are the  
 816 same to within  $10^{-7}$ ). (c) Standard deviation of  $\mathbf{X}'_a$  for AC07 ordering 1 and (d) ordering 2.  
 817 (e) The absolute difference between the serial analysis with ordering 1 and 2 from (c) and  
 818 (d). (f) The absolute difference between the EPS solution and ordering 1 from (c). . . . . 44

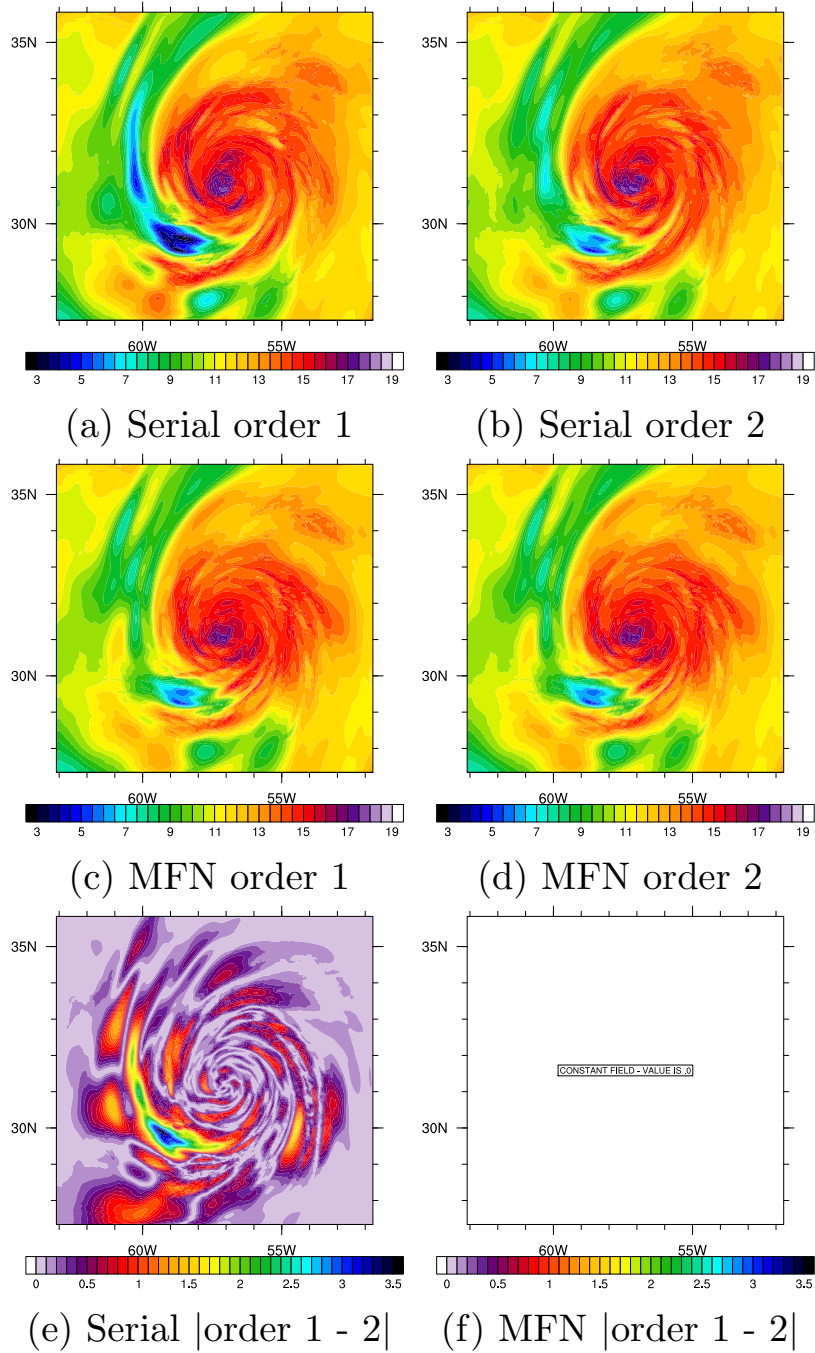
819 **Fig. 4.** (a) Speed increase of applying the MFN filter, including the time to calculate  $(\mathbf{E}|\mathbf{g})$  using  
 820 the matrix function approach and solve equation (1) as a function of number of processing  
 821 elements with the number of observations fixed at 17k. The speedup is nearly linear and is  
 822 dominated by the time applying  $\mathbf{C}_{x,Hx}$ . This should be compared with figure 6d) from S17  
 823 which likewise shows a nearly linear speed increase as a function of number of processors  
 824 during filter time. (b) Total speed increase of wall-time including disk reads and writes.  
 825 As the process is I/O bound, the total speed increase is sublinear. Compare with figure 6f)  
 826 from S17 which likewise shows a sub-linear increase (and even an eventual decrease) as a  
 827 function of total wall time due to degradation in parallel I/O performance. . . . . 45

828 **Fig. 5.** Scaling as a function of number of observations with 386 processors. The MFN approach  
 829 described in this paper appears to scale approximately linearly ( $y = 4.86 \times 10^{-2}x + 152$ ),  
 830 while the EPS scales consistent with a cubic fit ( $y = 4.43 \times 10^{-10}x^3 + 302$ ). The serial filter  
 831 of Anderson and Collins (2007) likewise scales linearly ( $y = 4.04 \times 10^{-2}x + 224.72$ ). Times  
 832 longer than 2500 seconds for the EPS solution are not shown. . . . . 46

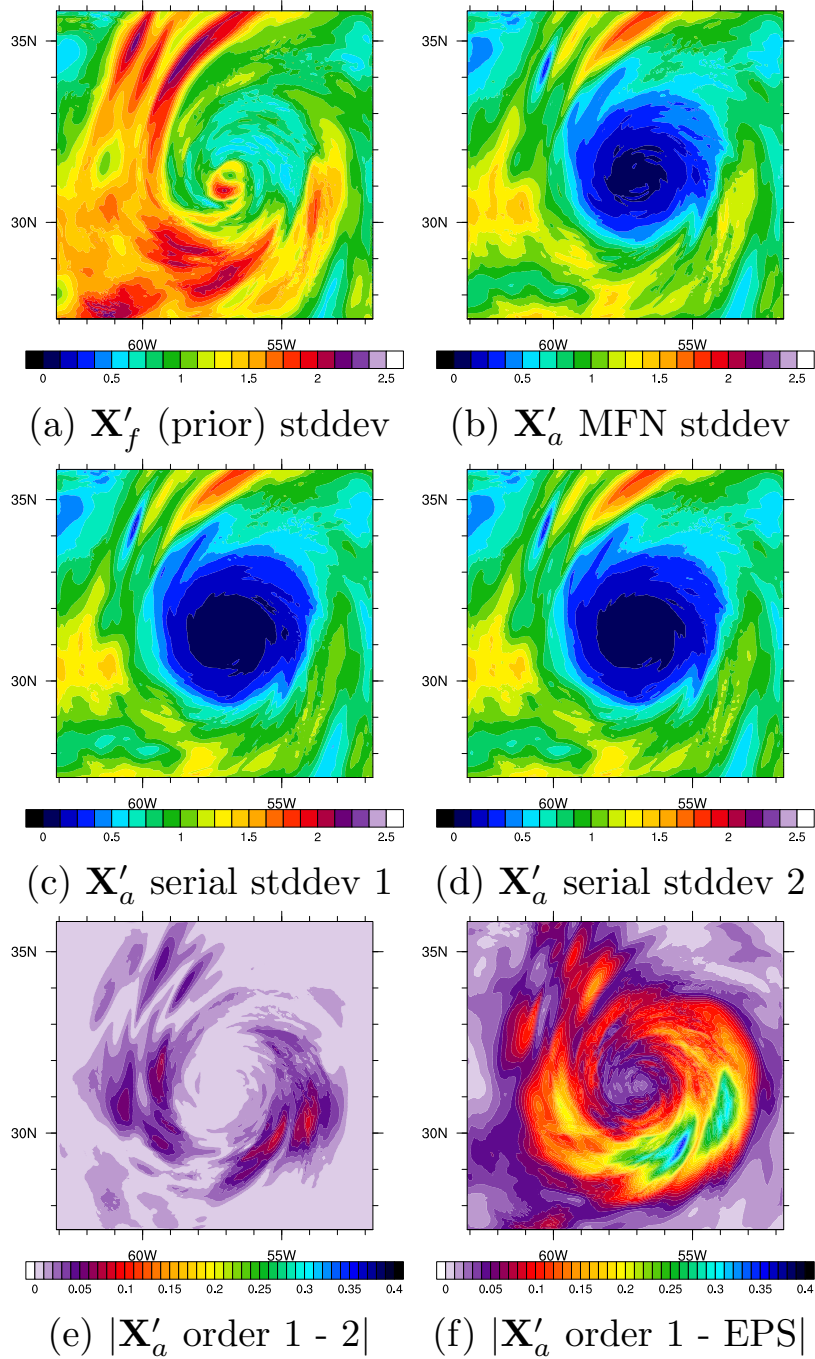
833 **Fig. 6.** Memory usage as a function of the number of observations with 386 processors. The EPS  
 834 scales cubically as predicted by theory, while the serial filter of Anderson and Collins (2007)  
 835 scales linearly in memory usage. The MFN approach apparently scales worse than linearly.  
 836 A matrix-free implementation of MFN improves memory scaling. . . . . 47



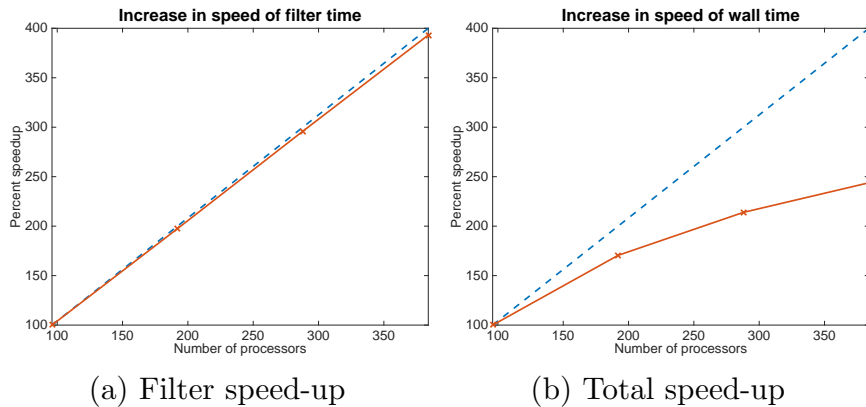
837 FIG. 1. Comparison between water vapor ( $\text{g kg}^{-1}$ ) at level 20 (of 60 total, corresponding to a height of  
 838 approximately 2.5 km) of the Hurricane Edouard single cycle case of Christophersen et al. (2017) with 15.2K  
 839 observations and  $L = 240$  as described in S17. Ten different random orderings of observations were used. (a)  
 840 The average of the ten AC07  $\bar{x}_a$  analyses. (b) The standard deviation of these ten AC07  $\bar{x}_a$  analyses. (c) The  
 841 average of the ten matrix function (MFN)  $\bar{x}_a$  analyses. (d) The standard deviation of the MFN analyses, which  
 842 is less than  $10^{-7}$  at all points. (e) The absolute difference between (a) and the EPS solution. (f) The absolute  
 843 difference between (c) and the EPS solution (also less than  $10^{-7}$  for all points).



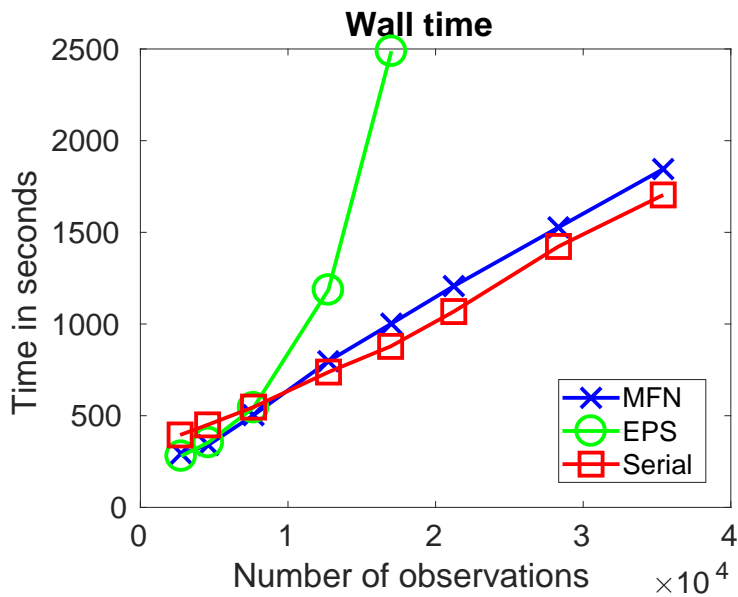
844 FIG. 2. Comparison between analyzed  $\bar{x}_a$  level 20 water vapor as in fig. 1 for two of the ten different random  
 845 orderings of observations. (a) The serial filter of Anderson and Collins (2007) with ordering 1 and (b) ordering  
 846 2. (c) MFN analyzed  $\bar{x}_a$  ordering 1. (d) MFN  $\bar{x}_a$  ordering 2. (e) The absolute value difference between (a) and  
 847 (b). (f) The difference between the two MFN orderings in (c) and (d), which is less than  $10^{-7}$ . The difference  
 848 between the MFN and EPS analysis for this case is also less than  $10^{-7}$  at all levels.



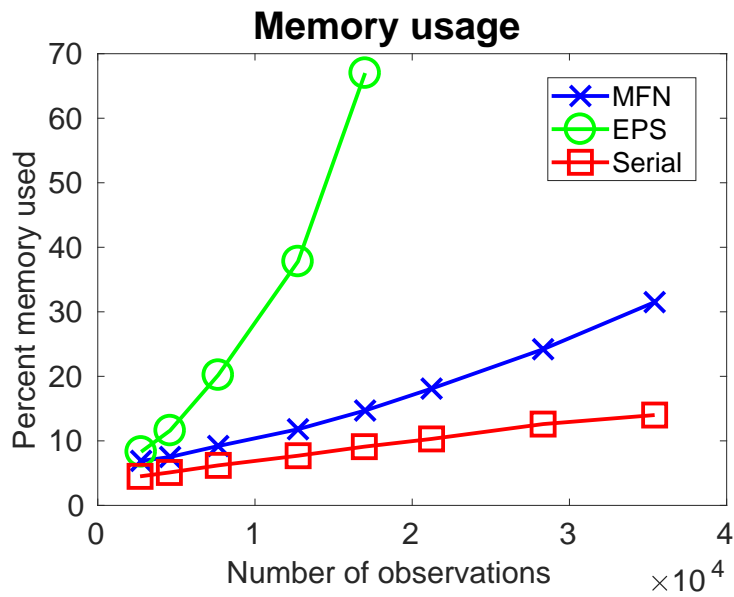
849 FIG. 3. Ensemble spread (i.e. standard deviations over the ensemble) of water vapor ( $\text{g kg}^{-1}$ ) at level 20 as  
850 in figures 1 and 2. Here the first two random orderings of observations were used as in fig. 2. (a) The standard  
851 deviation of the prior distribution  $\mathbf{X}'_f$  at this level. (b) The standard deviation of the MFN posterior distribution  
852  $\mathbf{X}'_a$  (ordering 1, 2, and the EPS solution are the same to within  $10^{-7}$ ). (c) Standard deviation of  $\mathbf{X}'_a$   
853 ordering 1 and (d) ordering 2. (e) The absolute difference between the serial analysis with ordering 1 and 2 from  
854 (c) and (d). (f) The absolute difference between the EPS solution and ordering 1 from (c).



855 FIG. 4. (a) Speed increase of applying the MFN filter, including the time to calculate  $(\mathbf{E}|\mathbf{g})$  using the matrix  
 856 function approach and solve equation (1) as a function of number of processing elements with the number of  
 857 observations fixed at 17k. The speedup is nearly linear and is dominated by the time applying  $\mathbf{C}_{x,Hx}$ . This  
 858 should be compared with figure 6d) from S17 which likewise shows a nearly linear speed increase as a function  
 859 of number of processors during filter time. (b) Total speed increase of wall-time including disk reads and writes.  
 860 As the process is I/O bound, the total speed increase is sublinear. Compare with figure 6f) from S17 which  
 861 likewise shows a sub-linear increase (and even an eventual decrease) as a function of total wall time due to  
 862 degradation in parallel I/O performance.



863 FIG. 5. Scaling as a function of number of observations with 386 processors. The MFN approach described  
 864 in this paper appears to scale approximately linearly ( $y = 4.86 \times 10^{-2}x + 152$ ), while the EPS scales consistent  
 865 with a cubic fit ( $y = 4.43 \times 10^{-10}x^3 + 302$ ). The serial filter of Anderson and Collins (2007) likewise scales  
 866 linearly ( $y = 4.04 \times 10^{-2}x + 224.72$ ). Times longer than 2500 seconds for the EPS solution are not shown.



867 FIG. 6. Memory usage as a function of the number of observations with 386 processors. The EPS scales  
 868 cubically as predicted by theory, while the serial filter of Anderson and Collins (2007) scales linearly in mem-  
 869 ory usage. The MFN approach apparently scales worse than linearly. A matrix-free implementation of MFN  
 870 improves memory scaling.